

RESEARCH ARTICLE | OCTOBER 15 2024

## Macrotransport of active particles in periodic channels and fields: Rectification and dispersion

Special Collection: 2024 JCP Emerging Investigators Special Collection

Zhiwei Peng  

 Check for updates

*J. Chem. Phys.* 161, 154101 (2024)

<https://doi.org/10.1063/5.0232614>



### Articles You May Be Interested In

KoopmanLab: Machine learning for solving complex physics equations

*APL Mach. Learn.* (September 2023)

Experimental realization of a quantum classification: Bell state measurement via machine learning

*APL Mach. Learn.* (September 2023)

# Macrotransport of active particles in periodic channels and fields: Rectification and dispersion

Cite as: J. Chem. Phys. 161, 154101 (2024); doi: 10.1063/5.0232614

Submitted: 9 August 2024 • Accepted: 29 September 2024 •

Published Online: 15 October 2024



View Online



Export Citation



CrossMark

Zhiwei Peng<sup>a)</sup> 

## AFFILIATIONS

Department of Chemical and Materials Engineering, University of Alberta, Edmonton, Alberta T6G 1H9, Canada

**Note:** This paper is part of the 2024 JCP Emerging Investigators Special Collection.

<sup>a)</sup>Author to whom correspondence should be addressed: [zhiwei.peng@ualberta.ca](mailto:zhiwei.peng@ualberta.ca)

## ABSTRACT

Transport and dispersion of active particles in structured environments, such as corrugated channels and porous media, are important for the understanding of both natural and engineered active systems. Owing to their continuous self-propulsion, active particles exhibit rectified transport under spatially asymmetric confinement. While progress has been made in experiments and particle-based simulations, a theoretical understanding of the effective long-time transport dynamics in spatially periodic geometries remains less developed. In this paper, we apply generalized Taylor dispersion theory to analyze the long-time effective transport dynamics of active Brownian particles (ABPs) in periodic channels and fields. We show that the long-time transport behavior is governed by an effective advection–diffusion equation. The derived macrotransport equations allow us to characterize the average drift and effective dispersion coefficient. For the case of ABPs subject to a no-flux boundary condition at the channel wall, we show that regardless of activity, the average drift is given by the net diffusive flux along the channel. For ABPs, their activity is the driving mechanism that sustains a density gradient, which ultimately leads to rectified motion along the channel. Our continuum theory is validated against direct Brownian dynamics simulations of the Langevin equations governing the motion of each ABP.

Published under an exclusive license by AIP Publishing. <https://doi.org/10.1063/5.0232614>

## I. INTRODUCTION

The transport of active particles in confined environments is important for the understanding of both natural and engineered active systems. Examples include upstream contamination of motile bacteria<sup>1,2</sup> and the use of micromotors for cargo delivery.<sup>3–5</sup> The interplay between self-propulsion, geometric confinement, and fluid flows often leads to interesting transport dynamics that are unattainable for passive Brownian systems.<sup>6,7</sup> Owing to their persistent self-propulsion, active particles accumulate at confining boundaries. When placed under a pressure-driven channel flow, they can migrate against the flow.

The accumulation of active particles at boundaries depends on the curvature.<sup>8–10</sup> When the obstacle or boundary exhibits spatial asymmetry, active motion can be rectified. For example, particle-based simulations and experiments have shown that swimming bacteria can power gears with asymmetric teeth.<sup>11–16</sup> When the asymmetric boundary is held fixed, active particles will then produce a net flux due to this ratchet effect.<sup>17–22</sup> Such rectified transport has been considered for active particles in a spatially periodic

channel (see Fig. 1 for a schematic). To achieve a non-zero net flux through the channel, the boundary of the channel unit cell must exhibit fore-aft asymmetry. Other geometries such as funnel arrays and periodic porous media with asymmetric pillars have also been considered.<sup>23–27</sup> In the absence of geometric confinement, one can also obtain rectification with spatially asymmetric ratchet potential fields.<sup>22,28–30</sup> For a review on ratchet effects in active systems, see the work of Reichhardt and Reichhardt.<sup>22</sup>

Previous works on the rectified transport of active particles through corrugated channels mainly focused on particle-based simulations. In such simulations, the Langevin equations of motion governing the evolution of the stochastic trajectories of active particles are numerically integrated in time. An appropriate ensemble average of the stochastic trajectories allows one to characterize the mean and mean-squared displacements, from which the average speed and dispersion coefficient can be calculated.

To complement previous simulation results, in this work, we develop a statistical mechanical description of the effective long-time longitudinal transport dynamics of active particles in spatially periodic geometries. We restrict our consideration to dilute

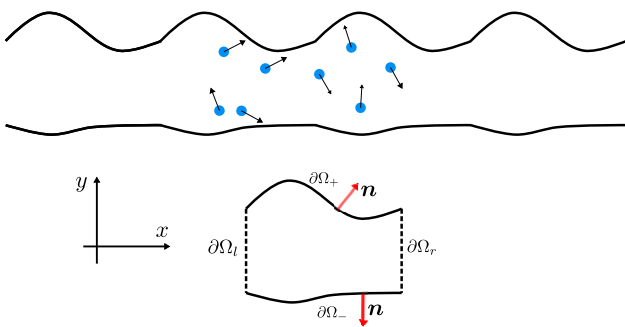


**FIG. 1.** Top: schematic of active Brownian particles in a periodic channel. The particles are treated as point particles in the text. Bottom: schematic of the unit cell ( $\Omega$ ) and its no-flux ( $\partial\Omega_w = \partial\Omega_+ \cup \partial\Omega_-$ ) and periodic ( $\partial\Omega_l \cup \partial\Omega_r$ ) boundaries. The unit outward normal vector of the channel walls is  $\mathbf{n}$ . The unit basis vector in the  $j$  direction of the Cartesian coordinate system is  $\mathbf{e}_j$  for  $j = \{x, y, \dots\}$ .

systems where only single particle dynamics are important. In addition, hydrodynamic interactions between the particle and the channel walls are neglected. With these assumptions, we adopt the active Brownian particle (ABP) model to describe the active dynamics (see Sec. II for details). Starting from the Smoluchowski equation governing the probability density distribution of an ABP in its position and orientation space, we derive a pair of so-called macrotransport equations that characterize the long-time transport dynamics. More specifically, these equations allow us to calculate the average drift velocity along the channel and the effective longitudinal dispersion coefficient at long times. We consider ABPs in periodic channels, spatially periodic fields, and a combination of geometric channel confinement and external fields.

The macrotransport theory developed here is a generalized Taylor dispersion theory (GTDT) for ABPs in spatially periodic geometries. In this context, one is concerned with the macroscopic dynamics that emerge after ABPs have passed through many copies of the unit cell. The macrotransport equations provide a bridge between the local dynamics and the macroscopic dynamics. The mathematical derivations follow closely those of Refs. 31 and 32.

For ABPs in a periodic channel in the absence of external flows and fields, we show that the average drift speed ( $U^{\text{eff}}$ ) along the channel at long times can be given by

$$U^{\text{eff}} = -D_T \left\langle \frac{\partial \rho_0}{\partial x} \right\rangle, \quad (1)$$

where  $D_T$  is the translational diffusivity of the ABP,  $\rho_0$  is the number density field,  $x$  is the longitudinal coordinate, and the angle brackets denote the cell average. Equation (1) is obtained for ABPs subject to a no-flux boundary condition at the wall. We note that activity (e.g., swim speed) does not appear explicitly in Eq. (1), which applies to both passive Brownian particles (PBPs) and ABPs. That is, regardless of activity, the drift is given by the net diffusive flux along the channel. For PBPs, the density field is spatially uniform and the drift vanishes. In the case of ABPs, their activity coupled to asymmetric confinement allows the system to maintain a density gradient at steady state, which ultimately leads to rectified transport. As shown by previous work, boundary conditions dictate the macrotransport

dynamics.<sup>24</sup> For active particles that obey an orientation-reflection condition (rule III in Ref. 24), no rectification is present.

Different from the drift speed  $U^{\text{eff}}$ , the swim speed provides a direct contribution to the longitudinal dispersion coefficient—the swim diffusivity modified by asymmetric confinement. In addition, fluctuation in the number density gives another contribution, which is also present for PBPs. In the general case where ABPs are under the influence of both geometric confinement and external fields (such as channel flow), the net swimming motion does contribute directly to the drift. In the main text, we contrast the different contributions to the drift and dispersion coefficient for cases including channel confinement, external fields, orienting fields, and activity landscapes.

This paper is organized as follows. In Sec. II, we introduce the Smoluchowski formulation and derive the macrotransport equations for ABPs in spatially periodic environments. We first provide a systematic derivation for the case of ABPs in periodic channels without external fields. We then characterize the average drift and the effective longitudinal dispersion, respectively, in Secs. II A and II B. Additional discussions on rectification and dispersion are provided in Sec. II C. In Sec. III A, we consider the macrotransport dynamics of ABPs in periodic potentials or fields without geometric confinement. We consider the effect of periodic orienting fields in the absence of channel confinement in Sec. III B. In Sec. III C, we discuss the combined effects of channel confinement and external fields. The spatially periodic activity landscape is considered in Sec. III D. In Sec. IV, we conduct asymptotic analyses in the limits of weak activity and nearly flat channels. In Sec. V, we apply our theory to characterize the macrotransport of ABPs in a corrugated channel and a one-dimensional substrate potential. We conclude our paper in Sec. VI.

## II. PROBLEM FORMULATION

Consider the transport of a dilute suspension of spherical ABPs in a quiescent fluid in a periodic channel (see Fig. 1). We assume that the radius of the ABPs is negligible compared to the minimum width of the channel and treat the ABPs as “point” particles. In the dilute limit, we further consider the one-particle probability distribution  $P(\mathbf{X}, \mathbf{q}, t)$  of finding an ABP at position  $\mathbf{X}$  with orientation  $\mathbf{q}$  ( $|\mathbf{q}| = 1$ ) at time  $t$ . The evolution of  $P$  satisfies the Smoluchowski equation,

$$\frac{\partial P}{\partial t} + \nabla_{\mathbf{X}} \cdot \mathbf{j}_T + \nabla_{\mathbf{R}} \cdot \mathbf{j}_R = 0, \quad (2)$$

where  $\nabla_{\mathbf{X}} = \partial/\partial \mathbf{X}$  and  $\nabla_{\mathbf{R}} = \mathbf{q} \times \partial/\partial \mathbf{q}$  are gradient operators in physical and orientation space, respectively. In (2), the translational flux  $\mathbf{j}_T$  and rotational flux  $\mathbf{j}_R$  are, respectively,

$$\mathbf{j}_T = U_s \mathbf{q} P - D_T \nabla_{\mathbf{X}} P, \quad (3a)$$

$$\mathbf{j}_R = -D_R \nabla_{\mathbf{R}} P. \quad (3b)$$

The spatial periodicity along the channel ( $x$  direction) allows us to relate the global position vector  $\mathbf{X}$  to the position vector  $\mathbf{x}$ , defined locally in a unit cell, via the relation

$$\mathbf{X} = jL \mathbf{e}_x + \mathbf{x}, \quad j \in \mathbb{Z}, \quad (4)$$

where  $L$  is the spatial periodicity or unit cell length and  $\mathbf{e}_x$  is the unit vector in the  $x$  direction. At the top ( $\partial\Omega_+$ ) and bottom channel walls ( $\partial\Omega_-$ ) of the unit cell, the no-flux condition is imposed,<sup>33</sup> giving

$$\mathbf{n} \cdot \mathbf{j}_T = 0, \quad \mathbf{x} \in \partial\Omega_w, \quad (5)$$

where  $\mathbf{n}$  is the unit outward normal vector of a boundary and  $\partial\Omega_w = \partial\Omega_+ \cup \partial\Omega_-$  (see Fig. 1 for a schematic of the periodic channel). With (4), one can then rewrite  $P(\mathbf{X}, \mathbf{q}, t)$  in terms of the sequence  $\{P_j(\mathbf{x}, \mathbf{q}, t), \forall j \in \mathbb{Z}\}$ , where  $P_j$  is the probability distribution within the cell  $j$ . In other words, to locate the particle in physical space, one can first identify the cell,  $j$ , in which the particle resides and then use the local position  $\mathbf{x}$  within this cell.

Taking the zeroth orientational moment of (2) gives a conservation equation for the number density,

$$\frac{\partial \rho}{\partial t} + \nabla_{\mathbf{X}} \cdot \mathbf{j}_{\rho} = 0, \quad (6a)$$

$$\mathbf{j}_{\rho} = U_s \mathbf{m} - D_T \nabla_{\mathbf{X}} \rho, \quad (6b)$$

where

$$\rho(\mathbf{X}, t) = \int_{\mathbb{S}} P(\mathbf{X}, \mathbf{q}, t) d\mathbf{q} \quad (7)$$

is the number density,

$$\mathbf{m}(\mathbf{X}, t) = \int_{\mathbb{S}} \mathbf{q} P(\mathbf{X}, \mathbf{q}, t) d\mathbf{q} \quad (8)$$

is the polar order, and  $\mathbb{S}$  denotes the unit sphere of orientations in  $d$  (e.g.,  $d = 2$  and 3) spatial dimensions. Unless otherwise specified, the derivation applies to both 2D and 3D. The “volume” of the orientation space is given by  $|\mathbb{S}| = \int_{\mathbb{S}} d\mathbf{q}$ . In 2D,  $|\mathbb{S}| = 2\pi$ ; in 3D,  $|\mathbb{S}| = 4\pi$ .

Because the channel is unbounded along the  $x$  direction, it is more convenient to work in Fourier space. To this end, we introduce the semidiscrete Fourier transform,<sup>34</sup>

$$\hat{f}(k) = L \sum_{j=-\infty}^{\infty} e^{-ikjL} f_j, \quad (9)$$

where  $k$  is the wavenumber,  $i$  ( $i^2 = -1$ ) is the imaginary unit, and  $f_j$  denotes the function  $f$  restricted to the unit cell  $j$ . We note that the transform is from  $j$  to  $k$ , and the local spatial coordinate  $\mathbf{x}$  is unchanged. To capture the long-time macrotransport dynamics, we write the derivative  $\partial/(\partial\mathbf{X})$  as  $\partial/(\partial\mathbf{x}) + \mathbf{e}_x \partial/[\partial(jL)]$ . At the macroscopic scale, the discrete cell indices can be effectively treated as a continuum. In Fourier space, the Smoluchowski equation (2) becomes

$$\frac{\partial \hat{P}}{\partial t} + (ik\mathbf{e}_x + \nabla) \cdot \hat{\mathbf{j}}_T + \nabla_R \cdot \hat{\mathbf{j}}_R = 0, \quad (10a)$$

$$\hat{\mathbf{j}}_T = U_s \mathbf{q} \hat{P} - D_T (ik\mathbf{e}_x + \nabla) \hat{P}, \quad (10b)$$

$$\hat{\mathbf{j}}_R = -D_R \nabla_R \hat{P}, \quad (10c)$$

where  $\hat{P} = \hat{P}(k, \mathbf{x}, \mathbf{q}, t)$  and  $\nabla = \partial/\partial\mathbf{x}$ . We note that the sequence of functions  $P_j$  reduces to a single function  $\hat{P}$  in Fourier space. That is,

the dependence on the cell index in real space transforms to a dependence on the wavenumber  $k$  in Fourier space. At long times, we impose periodic boundary conditions on the Fourier-transformed fields,<sup>31,32</sup>

$$\hat{P}(\mathbf{x}, \mathbf{q}, t) = \hat{P}(\mathbf{x} - Le_x, \mathbf{q}, t), \quad \mathbf{x} \in \partial\Omega_r, \quad (11a)$$

$$\nabla \hat{P}(\mathbf{x}, \mathbf{q}, t) = \nabla \hat{P}(\mathbf{x} - Le_x, \mathbf{q}, t), \quad \mathbf{x} \in \partial\Omega_r. \quad (11b)$$

Similarly, the number density Eq. (6) in Fourier space is given by

$$\frac{\partial \hat{\rho}}{\partial t} + (ik\mathbf{e}_x + \nabla) \cdot \hat{\mathbf{j}}_{\rho} = 0, \quad (12a)$$

$$\hat{\mathbf{j}}_{\rho} = U_s \hat{\mathbf{m}} - D_T (ik\mathbf{e}_x + \nabla) \hat{\rho}. \quad (12b)$$

Averaging (12) over the unit cell  $\Omega$ , we have

$$\frac{\partial \langle \hat{\rho} \rangle}{\partial t} + ik\mathbf{e}_x \cdot \langle \hat{\mathbf{j}}_{\rho} \rangle = 0, \quad (13a)$$

$$\langle \hat{\mathbf{j}}_{\rho} \rangle = U_s \langle \hat{\mathbf{m}} \rangle - D_T (ik\mathbf{e}_x \langle \hat{\rho} \rangle + \langle \nabla \hat{\rho} \rangle), \quad (13b)$$

where  $\langle (\cdot) \rangle = (1/|\Omega|) \int_{\Omega} (\cdot) d\mathbf{x}$  and  $|\Omega|$  is the volume (3D) or area (2D) of the unit cell. We note that  $\langle \hat{\rho} \rangle$  is a function of  $k$  and  $t$ ,  $\langle \hat{\rho} \rangle = \langle \hat{\rho} \rangle(k, t)$ . In deriving (13), we have applied the divergence theorem, the no-flux boundary conditions on the top and bottom walls, and the periodic condition (11) on the left and right edges of the unit cell (see Fig. 1). To relate  $\hat{P}$  to  $\langle \hat{\rho} \rangle$ , we define the “structure” function  $\hat{G}$  such that

$$\hat{P}(k, \mathbf{x}, \mathbf{q}, t) = \langle \hat{\rho} \rangle(k, t) \hat{G}(k, \mathbf{x}, \mathbf{q}, t). \quad (14)$$

By definition,  $\hat{G}$  satisfies the normalization,

$$\frac{1}{|\Omega|} \int_{\Omega} d\mathbf{x} \int_{\mathbb{S}} \hat{G} d\mathbf{q} = 1. \quad (15)$$

To derive an effective advection–diffusion equation for  $\langle \hat{\rho} \rangle$ , we first Taylor expand  $\hat{G}$  about  $k = 0$ , giving

$$\hat{G}(k, \mathbf{x}, \mathbf{q}, t) = g(\mathbf{x}, \mathbf{q}, t) + ik b(\mathbf{x}, \mathbf{q}, t) + O(k^2), \quad (16)$$

where  $g$  is the zero-wavenumber probability distribution (or the average field) and  $b$  is the displacement field.<sup>31,35–39</sup> From (14) and (16), we have

$$\frac{\hat{\rho}}{\langle \hat{\rho} \rangle} = \rho_0 + ik \rho_1 + O(k^2), \quad (17a)$$

$$\frac{\hat{\mathbf{m}}}{\langle \hat{\rho} \rangle} = \mathbf{m}_0 + ik \mathbf{m}_1 + O(k^2), \quad (17b)$$

where

$$\rho_0 = \int_{\mathbb{S}} g d\mathbf{q} \quad \text{and} \quad \rho_1 = \int_{\mathbb{S}} b d\mathbf{q} \quad (18)$$

and  $\mathbf{m}_0$  and  $\mathbf{m}_1$  are similarly defined. We note that an expansion similar to (17) can be written for any orientational moment of

$\hat{\rho}$ . Inserting (17) into (13), one can obtain an effective long-time advection–diffusion equation for  $\langle \hat{\rho} \rangle$  in Fourier space,

$$\frac{\partial \langle \hat{\rho} \rangle}{\partial t} + ik U^{\text{eff}} \langle \hat{\rho} \rangle + k^2 D^{\text{eff}} \langle \hat{\rho} \rangle = 0, \quad (19)$$

where the average drift and effective longitudinal dispersion coefficients are, respectively, given by

$$U^{\text{eff}} = U_s \mathbf{e}_x \cdot \langle \mathbf{m}_0 \rangle - D_T \mathbf{e}_x \cdot \langle \nabla \rho_0 \rangle, \quad (20a)$$

$$D^{\text{eff}} = D_T - U_s \mathbf{e}_x \cdot \langle \mathbf{m}_1 \rangle + D_T \mathbf{e}_x \cdot \langle \nabla \rho_1 \rangle. \quad (20b)$$

In writing (19), it is understood that higher-order terms in  $k$  are truncated since they do not contribute to either the drift or dispersion. We emphasize that (19) does not capture the short-time or transient dynamics. In the context of GTDT, the transport regime prior to the asymptotically long-time regime is often referred to as the pre-asymptotic regime.<sup>40,41</sup>

Subtracting (13) multiplied by  $\hat{G}$  from (10), we obtain

$$\begin{aligned} \frac{\partial \hat{G}}{\partial t} + i k \mathbf{e}_x \cdot \left[ U_s \left( \mathbf{q} - \frac{\langle \mathbf{m} \rangle}{\langle \hat{\rho} \rangle} \right) \hat{G} - D_T \left( \nabla \hat{G} - \frac{\langle \nabla \hat{\rho} \rangle}{\langle \hat{\rho} \rangle} \hat{G} \right) \right] \\ + \nabla \cdot (U_s \mathbf{q} \hat{G} - D_T i k \mathbf{e}_x \hat{G} - D_T \nabla \hat{G}) - D_R \nabla_R^2 \hat{G} = 0. \end{aligned} \quad (21)$$

The no-flux condition (5) is written as

$$\mathbf{n} \cdot [U_s \mathbf{q} \hat{G} - D_T (i k \mathbf{e}_x + \nabla) \hat{G}] = 0, \quad \mathbf{x} \in \partial \Omega_w. \quad (22)$$

In the  $x$  direction,  $\hat{G}$  satisfies the periodic conditions [see (11)].

## A. The average field and the average drift

Inserting expansion (16) into (21), one obtains at  $O(1)$  the governing equation

$$\frac{\partial g}{\partial t} + \nabla \cdot (U_s \mathbf{q} g - D_T \nabla g) - D_R \nabla_R^2 g = 0. \quad (23)$$

The no-flux condition is given by

$$\mathbf{n} \cdot (U_s \mathbf{q} g - D_T \nabla g) = 0, \quad \mathbf{x} \in \partial \Omega_w, \quad (24)$$

and the periodic conditions (11) require

$$g(\mathbf{x}, \mathbf{q}, t) = g(\mathbf{x} - L \mathbf{e}_x, \mathbf{q}, t), \quad \mathbf{x} \in \partial \Omega_r, \quad (25a)$$

$$\nabla g(\mathbf{x}, \mathbf{q}, t) = \nabla g(\mathbf{x} - L \mathbf{e}_x, \mathbf{q}, t), \quad \mathbf{x} \in \partial \Omega_r. \quad (25b)$$

Finally, from (15), we have the conservation of particles given by

$$\frac{1}{|\Omega|} \int_{\Omega} d\mathbf{x} \int_S g d\mathbf{q} = 1. \quad (26)$$

Equations (23)–(26) fully specify the problem at leading order, i.e.,  $O(1)$ . With  $g$ , one can then evaluate the orientational moments  $\rho_0$  and  $\mathbf{m}_0$ , from which the average drift can be determined using (20a).

The zeroth moment of  $g$ , or the number density, is governed by

$$\frac{\partial \rho_0}{\partial t} + \nabla \cdot (U_s \mathbf{m}_0 - D_T \nabla \rho_0) = 0, \quad (27a)$$

$$\mathbf{n} \cdot (U_s \mathbf{m}_0 - D_T \nabla \rho_0) = 0, \quad \mathbf{x} \in \partial \Omega_w, \quad (27b)$$

and the periodic conditions follow from (25). The first moment of  $g$  (the polar order  $\mathbf{m}_0$ ) satisfies the equation

$$\frac{\partial \mathbf{m}_0}{\partial t} + \nabla \cdot \left[ U_s \left( \mathbf{Q}_0 - \frac{\rho_0 \mathbf{I}}{d} \right) - D_T \nabla \mathbf{m}_0 \right] + (d-1) D_R \mathbf{m}_0 = \mathbf{0}, \quad (28)$$

where

$$\mathbf{Q}_0 = \int_S (\mathbf{q} \mathbf{q} - \mathbf{I}/d) g d\mathbf{q} \quad (29)$$

is the nematic order and  $\mathbf{I}$  is the identity tensor. Using the no-flux and periodic conditions, one can show that

$$\frac{\partial \langle \mathbf{m}_0 \rangle}{\partial t} + (d-1) D_R \langle \mathbf{m}_0 \rangle = 0. \quad (30)$$

Any initial polar order would decay to zero exponentially fast due to rotary diffusion:<sup>42</sup>  $\langle \mathbf{m}_0 \rangle \rightarrow \mathbf{0}$  as  $t \rightarrow \infty$ . From this, we see that the self-advective (or swimming) contribution to the average drift in (20a) vanishes at long times. Using the divergence theorem and periodic conditions, we have

$$U^{\text{eff}} = -D_T \mathbf{e}_x \cdot \langle \nabla \rho_0 \rangle = -\frac{D_T}{|\Omega|} \mathbf{e}_x \cdot \int_{\partial \Omega_w} \mathbf{n} \rho_0 dS, \quad (31)$$

where  $dS$  is the surface element in 3D and line element in 2D and  $\mathbf{n}$  is the unit normal vector of the boundary that points out of the domain  $\Omega$ .

In deriving (31), the swim speed is taken to be a constant. If the swim speed depends on the local position  $\mathbf{x}$ ,  $U_s = U_s(\mathbf{x})$ , the average drift should be written as  $U^{\text{eff}} = \mathbf{e}_x \cdot \langle U_s \mathbf{m}_0 \rangle - D_T \mathbf{e}_x \cdot \langle \nabla \rho_0 \rangle$ . In contrast to (20a), the swim speed needs to be included in the averaging procedure. At long times, while the net polar order still vanishes, the swim flux  $\langle U_s \mathbf{m}_0 \rangle$  does not necessarily vanish. With a position-dependent swim speed, the average drift has contributions from both the net swim flux and the diffusive flux.

Equation (31) can be deduced from the momentum balance of the particle phase in a unit cell. To see this, consider the micromechanical equation of motion of an active particle,<sup>43</sup> which is given by

$$\mathbf{0} = -\zeta \mathbf{U} + \mathbf{F}^{\text{swim}} + \mathbf{F}^B + \mathbf{F}^{\text{ext}} + \mathbf{F}^P, \quad (32)$$

where the swimming motion is driven by the swim force,  $\mathbf{F}^{\text{swim}} = \zeta U_s \mathbf{q}$ ,  $\zeta$  is the drag coefficient (recall that hydrodynamic interactions are absent),  $\mathbf{F}^B$  is the fluctuating Brownian force,  $\mathbf{F}^{\text{ext}}$  is the total external force on the particle,  $\mathbf{F}^P$  is the particle–particle interactive or collisional force, and  $\mathbf{U}$  is the instantaneous velocity of the particle. In the dilute limit, summing over all particles leads to the global force balance  $\zeta \langle \mathbf{U} \rangle = \mathbf{F}^w$ , where  $\mathbf{F}^w$  is the force that the top and bottom walls exert on the particles. We note that in writing this average

relation, we have used the fact that the net polar order vanishes [see (30)]. The force due to the wall is given by<sup>8,44</sup>

$$\mathbf{F}^w = - \int_{\partial\Omega_w} \rho k_B T \mathbf{n} dS, \quad (33)$$

where we have a minus sign because the integral (without the minus sign) is the net force the particles exert on the wall,  $k_B T$  is the thermal energy, and  $\rho k_B T$  is the osmotic pressure.<sup>44</sup> Using the Stokes–Einstein–Sutherland relation,  $\zeta D_T = k_B T$ , we arrive at the statement that  $U^{\text{eff}} = \langle \mathbf{U} \rangle \cdot \mathbf{e}_x = F_x^w / \zeta = -D_T \mathbf{e}_x \cdot \int_{\partial\Omega_w} \mathbf{n} \rho dS$ . Finally,  $\rho$  here is dimensional and can be related to  $\rho_0$  via  $\rho = \rho_0 / |\Omega|$ . As a result, one obtains precisely (31) from the momentum balance. The particles exhibit net motion simply to obey the conservation of momentum. Put differently, the channel walls can direct active particles and achieve autonomous directed motion from otherwise random active motion observed in free space. This is the so-called rectification or ratcheting of active Brownian motion.

It is clear that (31) applies to both active and passive Brownian motion, just like (33) for the wall force. One may be tempted to think that the average polar order multiplied by the swim speed  $U_s$  contributes *directly* to the drift velocity. As seen from the discussion leading from (20a)–(31), this is not the case; the net polar order vanishes. The only contribution—regardless of activity—is from the diffusive motion driven by the net density gradient. For passive Brownian particles, the density is uniform, and we do not observe an average drift. When activity is present, a density gradient can be generated; this is the well-known phenomenon of boundary accumulation of active particles.<sup>8,43,45–49</sup> In a channel with a fore-aft asymmetric boundary, the accumulation or density varies along the channel as a result of curvature variation.<sup>10</sup> While the net polar order vanishes, it contributes *indirectly* to the drift by driving the density out of equilibrium [see (27)] and maintaining a steady-state density gradient. Ultimately, this process gives rise to net drift or rectified motion. For passive Brownian particles, this intrinsic driving force is absent, and rectification is often achieved by applying external forces that bias and direct particles.<sup>50–52</sup>

Rectification allows us to harness the otherwise random—albeit active—motion of active particles to generate directed motion or perform useful work. While our focus here is on the autonomous macrotransport of active particles in channels, one can also achieve directed motion of a water permeable container that encapsulates active particles.<sup>53</sup> In exterior problems, objects immersed in an active bath are shown to exhibit spontaneous and directed rotation.<sup>12–14,54</sup> For a review on ratchet effects in active matter, see the work of Reichhardt and Reichhardt.<sup>22</sup>

We note that (31) was derived by Yariv and Schnitzer.<sup>55</sup> In their work, the average drift was considered in real (or physical) space instead of in Fourier space. Indeed, one may drop the dependence on the global coordinate  $jL$  from the outset and assume periodic conditions on  $P$ , which leads directly to (23). The average drift can then be obtained by averaging the translational flux for the density given in (27). This real-space approach is the leading-order moment in the so-called Aris's method of moments in the context of Taylor dispersion.<sup>56–61</sup> One can continue to higher order moments and obtain, for example, the effective longitudinal dispersion coefficient; this was not considered in the work of Yariv and Schnitzer.<sup>55</sup> We note that Aris's method of moments and the Fourier approach lead

to the same drift and dispersion coefficients in general macrotransport processes. We find it more intuitive to work in Fourier space since the wavenumber  $k$  provides a natural parameter for ordering the drift and dispersion coefficient [see, for example, Eq. (19)].

## B. The displacement field and the effective dispersion

Equation (21) at  $O(k)$  gives

$$\frac{\partial b}{\partial t} + \nabla \cdot (U_s \mathbf{q} b - D_T \nabla b) - D_R \nabla^2 b = 2D_T \frac{\partial g}{\partial x} + (U^{\text{eff}} - U_s q_x) g, \quad (34)$$

where  $q_x = \mathbf{q} \cdot \mathbf{e}_x$ . The boundary condition at the top and bottom of the unit cell is given by

$$\mathbf{n} \cdot (U_s \mathbf{q} b - D_T \nabla b) = \mathbf{n} \cdot \mathbf{e}_x D_T g, \quad \mathbf{x} \in \partial\Omega_w. \quad (35)$$

In the  $x$  direction,  $b$  obeys the periodic conditions similar to (25). The conservation condition (15) implies that

$$\int_{\Omega} d\mathbf{x} \int_S b d\mathbf{q} = 0. \quad (36)$$

Note that the operators on the left-hand side of (34) are the same as (23) and the displacement field is driven by the  $g$  field. More specifically, it is driven by a diffusive flux plus the deviation of the swimming motion from the mean drift. We also note that the boundary condition (35) is also non-homogeneous.

To determine the effective dispersion coefficient, the number density and polar order of  $b$  are needed. Taking the zeroth orientational moment of (34) gives the equation for  $\rho_1$ ,

$$\frac{\partial \rho_1}{\partial t} + \nabla \cdot (U_s \mathbf{m}_1 - D_T \nabla \rho_1) = 2D_T \frac{\partial \rho_0}{\partial x} + U^{\text{eff}} \rho_0 - U_s m_{0,x}, \quad (37)$$

where  $m_{0,x} = \mathbf{m}_0 \cdot \mathbf{e}_x$ . The boundary condition on the wall follows from (35) and is given by

$$\mathbf{n} \cdot (U_s \mathbf{m}_1 - D_T \nabla \rho_1) = D_T \rho_0 \mathbf{n} \cdot \mathbf{e}_x, \quad \mathbf{x} \in \partial\Omega_w. \quad (38)$$

The total density at  $O(k)$  is zero,  $\int_{\Omega} \rho_1 d\mathbf{x} = 0$ . Using (38) and the periodic condition, one can show that the average of (37) leads to the equation  $0 = D_T \mathbf{e}_x \cdot (\nabla \rho_0) + U^{\text{eff}}$ , which is consistent with (31). The governing equation for the polar order is given by

$$\begin{aligned} \frac{\partial \mathbf{m}_1}{\partial t} + \nabla \cdot \left[ U_s \left( \mathbf{Q}_1 + \frac{1}{d} \rho_1 \mathbf{I} \right) - D_T \nabla \mathbf{m}_1 \right] + (d-1) D_R \mathbf{m}_1 \\ = 2D_T \frac{\partial \mathbf{m}_0}{\partial x} + U^{\text{eff}} \mathbf{m}_0 - U_s \left( \mathbf{Q}_0 + \frac{1}{d} \rho_0 \mathbf{I} \right) \cdot \mathbf{e}_x. \end{aligned} \quad (39)$$

At the top and bottom walls,  $\mathbf{x} \in \partial\Omega_w$ , we have

$$\mathbf{n} \cdot \left[ U_s \left( \mathbf{Q}_1 + \frac{1}{d} \rho_1 \mathbf{I} \right) - D_T \nabla \mathbf{m}_1 \right] = D_T \mathbf{n} \cdot \mathbf{e}_x \mathbf{m}_0. \quad (40)$$

The polar order is also periodic in the  $x$  direction.

Averaging (39) in the unit cell at long times gives

$$\langle \mathbf{m}_1 \rangle = -\frac{\ell}{d(d-1)} \mathbf{e}_x + \frac{\delta^2}{d-1} \langle \nabla \cdot (\mathbf{e}_x \mathbf{m}_0) \rangle, \quad (41)$$

where we have used the relations  $\langle \mathbf{m}_0 \rangle = \mathbf{0}$  [see (30)] and  $\langle \mathbf{Q}_0 \rangle = \mathbf{0}$ ,<sup>62</sup>  $\delta = \sqrt{D_T \tau_R}$  is the microscopic length, and  $\ell = U_s \tau_R$  is the run (or persistence) length. Inserting (41) into (20b), we have

$$D^{\text{eff}} = D_0^{\text{eff}} - \frac{U_s \delta^2}{d-1} \mathbf{e}_x \mathbf{e}_x : (\nabla \mathbf{m}_0) + D_T \mathbf{e}_x \cdot (\nabla \rho_1), \quad (42)$$

where  $D_0^{\text{eff}} = D_T + D_0^{\text{swim}}$  is the effective diffusivity of an ABP in free space (or the effective longitudinal diffusivity in a flat channel<sup>39</sup>) and  $D_0^{\text{swim}} = U_s^2 \tau_R / [d(d-1)]$  is the swim diffusivity. Note that  $D_0^{\text{eff}}$  emerges naturally from the above consideration and the effect of the channel confinement appears as additional contributions (or corrections) in (42). We also remark that  $\rho_1$  has units of length, which follows from expansion (16).

### C. Macrotransport of active particles in periodic channels

Equations (31) and (42) are the main results of this paper. To calculate the average drift in (31), one needs to solve for the average field  $g$  using (23)–(26) and then take the zeroth orientational moment to obtain  $\rho_0$ . Similarly, the longitudinal dispersion depends on the solution to the displacement field  $b$ , which is governed by (34)–(36). Equations (31) and (42) and the aforementioned governing equations for the average and displacement fields provide a complete description of macrotransport of active particles in periodic channels. We remark that no assumptions regarding the geometry of the channel unit cell have been made and no approximations have been made in deriving the macrotransport equations beyond the Smoluchowski equation (2). Therefore, these equations apply to generic periodic channels and provide an exact characterization of the macrotransport of active (or passive) particles.

In (31), we have shown that the average drift results from the net diffusive transport along the channel. For passive particles regardless of the channel geometry, the density gradient vanishes and the average drift is zero. For active particles, if the channel walls are flat and parallel, one can see that the net flux vanishes due to symmetry. As a result, for passive particles, external steady and/or oscillatory driving forces are often employed in order to achieve rectified transport; for active particles, however, fore-aft asymmetric channel confinement alone is able to drive a nonzero average drift. That is, active particles under appropriate confinement exhibit *autonomous* rectification.

In addition to the average drift or rectified transport, we also derived the long-time effective longitudinal dispersion coefficient, as given by (42). For passive particles,  $U_s \equiv 0$ , one can readily show that  $g = 1/|\mathbb{S}|$ ,  $\rho_0 = 1$ , and  $\mathbf{m}_0 = \mathbf{0}$ . From (37) and (38), we then have

$$\nabla^2 \rho_1 = 0, \quad (43a)$$

$$\mathbf{n} \cdot \nabla \rho_1 = -\mathbf{n} \cdot \mathbf{e}_x, \quad \mathbf{x} \in \partial \Omega_w. \quad (43b)$$

From (42), for passive particles, we obtain

$$\frac{D_{\text{passive}}^{\text{eff}}}{D_T} = 1 + \left( \frac{\partial \rho_1}{\partial x} \right). \quad (44)$$

In the absence of activity, one only needs to solve the Laplace equation for  $\rho_1$  subject to a Neumann boundary condition on  $\partial \Omega_w$  and

periodicity in  $x$ . While channel confinement cannot give rise to rectified transport of passive particles, it modifies the dispersion coefficient. As noted earlier, regardless of activity, the average drift is given by the net diffusive transport—activity plays a role by driving the density out of equilibrium. This is not the case for the dispersion coefficient [see (44) and (42)]. Compared to the passive result (44), the active result in (42) has an additional contribution due to the fluctuations in the swimming motion or polar order. The fluctuations in swimming motion manifest as a swim diffusivity. Because of (41), this swimming contribution can be given by the undisturbed swim diffusivity and the additional contribution from the confinement.

While our aim was to derive a macrotransport theory for active particles in periodic (nonflat) channels, we can recover the transport problem of active particles in flat channels. To this end, we first note that for flat channels, the unit cell reduces to a rectangular domain and the width  $L$  along the channel can be arbitrarily chosen. For flat channels, the average and displacement fields do not depend on  $x$ . The average field equation (23) reduces to

$$\frac{\partial}{\partial y} \left( U_s q_y g - D_T \frac{\partial g}{\partial y} \right) - D_R \nabla_R^2 g = 0, \quad (45)$$

and the no-flux condition is  $U_s q_y g - D_T \frac{\partial g}{\partial y} = 0$  at  $y = \pm H$ . Here, we have assumed that the flat channel has a transverse width of  $2H$  with the top and bottom walls, respectively, located at  $y = H$  and  $y = -H$ . Because the wall normal  $\mathbf{n} = \pm \mathbf{e}_y$ , from (31), we see that  $U^{\text{eff}} = 0$ , as expected. Equation (45) governs the distribution of active particles confined between two flat plates, which is a well-studied problem. Notably, due to their self-propulsion, active particles accumulate at the wall. The displacement field equation (34) can be written as

$$\frac{\partial}{\partial y} \left( U_s q_y b - D_T \frac{\partial b}{\partial y} \right) - D_R \nabla_R^2 b = -U_s q_x g. \quad (46)$$

The boundary conditions are given by

$$U_s q_y b - D_T \frac{\partial b}{\partial y} = 0, \quad y = \pm H. \quad (47)$$

We note that the boundary conditions are homogeneous [cf. (35)] since  $\mathbf{n} \cdot \mathbf{e}_x = 0$ . From (42), it is clear that  $D^{\text{eff}} = D_0^{\text{eff}}$ . For flat channels, we see that the average drift is zero and the longitudinal dispersion equals that in free space.<sup>39</sup> In the presence of Poiseuille flow through flat channels, active particles are shown to exhibit upstream swimming and the longitudinal dispersion coefficient varies non-monotonically as a function of the flow speed.<sup>39</sup> In the presence of such flows, Eqs. (45) and (46) need to include the appropriate flow terms; similarly, additional contributions to the drift and dispersion from the background flow need to be considered (see Ref. 39).

In formulating the macrotransport equations, we took as an example a channel with two separate walls (see Fig. 1). We note that this is only for concreteness, and the derived equations apply equally well to a tube with periodically varying cross section. The only modification is that the no-flux portion of the unit cell boundary ( $\partial \Omega_w$ ) is now a single continuous surface instead of two separate walls.

Finally, we note that our formulation can also be extended to the transport of active particles in periodic porous media or

substrate.<sup>60,63–66</sup> In the work of Alonso-Matilla *et al.*,<sup>60</sup> Aris's moment method (real space) is used to study the drift and dispersion of active particles in flows through periodic porous media. We note that in a regular lattice of pillars, one needs to take the semidiscrete Fourier transform in all Cartesian directions (see Sec. III A for an example). The wall condition is now applied at the interior boundary of the unit cell (the surface of the pillar), and at the outer sides, periodic conditions apply. If the pillars are fore-aft asymmetric, rectified transport in porous media can also be achieved.<sup>26,27</sup>

### III. MACROTRANSPORT IN PERIODIC FIELDS

#### A. Periodic potentials or external fields

In the absence of confining asymmetric channels, directed transport of active particles can be achieved using asymmetric external fields or potentials.<sup>22,37,67,68</sup> In symmetric potential fields, the dispersion behavior of active particles is also non-trivial.<sup>31,69</sup> We consider the external force  $\mathbf{F}^{\text{ext}}$  to be spatially periodic such that  $\mathbf{F}^{\text{ext}}(\mathbf{x} + \mathbf{L}, t) = \mathbf{F}^{\text{ext}}(\mathbf{x}, t)$ , where  $\mathbf{L} = \sum_{j=1}^d z_j L_j \mathbf{e}_j$  (to be consistent with our notation,  $\mathbf{e}_1 = \mathbf{e}_x$ ,  $\mathbf{e}_2 = \mathbf{e}_y$ , etc.), with  $L_j$  being the periodicity and  $z_j \in \mathbb{Z}$  being the cell index in the  $j$  direction, respectively. We note that the force may be applied directly or derived from a periodic potential. Furthermore,  $\mathbf{F}^{\text{ext}}$  may also be time periodic with period  $T$ ,  $\mathbf{F}^{\text{ext}}(\mathbf{x}, t+T) = \mathbf{F}^{\text{ext}}(\mathbf{x}, t)$ , in which case an additional time average over a period  $T$  is needed to calculate the average drift and effective dispersion. In the Smoluchowski equation (2), we only need to include an additional translational flux term due to the external force given by  $\mathbf{U}^{\text{ext}} g$ , with  $\mathbf{U}^{\text{ext}} = \mathbf{F}^{\text{ext}}/\zeta$ .

The Fourier transform is now carried out in all directions. Instead of the scalar wavenumber  $k$ , we have the wave vector  $\mathbf{k}$  and the displacement field is a vector field. As a result, the small wavenumber expansion is  $\hat{g} = g + i\mathbf{k} \cdot \mathbf{b} + O(k^2)$ , where  $k$  is the norm of  $\mathbf{k}$ . Because the remaining derivation is similar to that in a periodic channel, in the following, we only summarize the main results. For details of the derivation, see the [supplementary material](#).

One can show that the average field is governed by

$$\frac{\partial g}{\partial t} + \nabla \cdot (U_s \mathbf{q} g + \mathbf{U}^{\text{ext}} g - D_T \nabla g) - D_R \nabla_R^2 g = 0, \quad (48)$$

where  $g$  is spatially periodic. The average drift is written as

$$\mathbf{U}^{\text{eff}} = \langle \mathbf{U}^{\text{ext}} \rho_0 \rangle. \quad (49)$$

The average polar order  $\langle \mathbf{m}_0 \rangle$  remains zero at long times in the presence of the external force. More importantly, we note that the diffusive term  $-D_T \langle \nabla \rho_0 \rangle$  vanishes due to spatial periodicity of the fields [cf. (31)]. The only contribution to the drift is from the external driving force,  $\langle \mathbf{U}^{\text{ext}} \rho_0 \rangle$ . The conservation condition (26) remains unchanged.

The displacement field satisfies the equation

$$\begin{aligned} \frac{\partial \mathbf{b}}{\partial t} + \nabla \cdot (U_s \mathbf{q} \mathbf{b} + \mathbf{U}^{\text{ext}} \mathbf{b} - D_T \nabla \mathbf{b}) - D_R \nabla_R^2 \mathbf{b} \\ = 2D_T \nabla g + (\mathbf{U}^{\text{eff}} - U_s \mathbf{q} - \mathbf{U}^{\text{ext}}) g \end{aligned} \quad (50)$$

and spatial periodicity. Because  $\mathbf{b}$  is a vector field, the “density” is a vector field,  $\rho_1 = \int_S \mathbf{b} d\mathbf{q}$ , and the polar order is a second-order tensor,  $\mathbf{m}_1 = \int_S \mathbf{b} \mathbf{q} d\mathbf{q}$ . In the presence of the external force, the effective dispersion tensor reads

$$\mathbf{D}^{\text{eff}} = D_T \mathbf{I} - U_s \langle \mathbf{m}_1 \rangle - \langle \mathbf{U}^{\text{ext}} \rho_1 \rangle, \quad (51)$$

where we have used the fact that  $\langle \nabla \rho_1 \rangle = 0$ . Following the procedure outlined in Sec. II B (see the [supplementary material](#)), one can show that at long times,

$$\langle \mathbf{m}_1 \rangle = -\frac{\ell}{d(d-1)} \mathbf{I} - \frac{\tau_R}{d-1} \langle \mathbf{U}^{\text{ext}} \mathbf{m}_0 \rangle. \quad (52)$$

From (51), we then have

$$\mathbf{D}^{\text{eff}} = D_0^{\text{eff}} \mathbf{I} + \frac{\ell}{d-1} \langle \mathbf{U}^{\text{ext}} \mathbf{m}_0 \rangle - \langle \mathbf{U}^{\text{ext}} \rho_1 \rangle. \quad (53)$$

We note that (53) and (51) are equivalent. Here, just like the drift, the driving force gives a direct contribution to the dispersion tensor,  $-\langle \mathbf{U}^{\text{ext}} \rho_1 \rangle$ . Compared to the free diffusion tensor  $D_0^{\text{eff}} \mathbf{I}$ , the external force drives additional density fluctuations, which ultimately affects the dispersion tensor. In contrast to channel confinement, the gradients of  $\mathbf{m}_0$  and  $\rho_1$  do not contribute to the dispersion.

Next, consider the simple case in which the external force is only a function of  $x$  and time  $t$ ,  $\mathbf{U}^{\text{ext}} = \mathbf{U}^{\text{ext}}(x, t)$ . That is, the force is invariant in the transverse directions. In this case, one can integrate out the transverse coordinates to obtain

$$\frac{\partial g}{\partial t} + \frac{\partial}{\partial x} \left( U_s q_x g + U_x^{\text{ext}} g - D_T \frac{\partial g}{\partial x} \right) - D_R \nabla_R^2 g = 0, \quad (54)$$

where  $g = g(x, \mathbf{q}, t) = g(x + L, \mathbf{q}, t)$ . As a result, the average drift in the  $x$  direction becomes

$$U_x^{\text{eff}} = \langle U_x^{\text{ext}} \rho_0 \rangle, \quad (55)$$

where the unit cell is 1D,  $\Omega = \{x | 0 \leq x \leq L\}$ , and  $\langle \cdot \rangle = (1/L) \int_0^L \langle \cdot \rangle dx$ . The average drift in the transverse direction is

$$\mathbf{U}_{\perp}^{\text{eff}} = (\mathbf{I} - \mathbf{e}_x \mathbf{e}_x) \cdot \mathbf{U}^{\text{eff}} = \langle \mathbf{U}_{\perp}^{\text{ext}} \rho_0 \rangle. \quad (56)$$

To understand this formula, consider a periodic driving force that gives  $\mathbf{U}^{\text{ext}} = U_{\parallel}(x, t) \mathbf{e}_x + U_{\perp} \mathbf{e}_y$ , where  $U_{\parallel}$  is  $L$ -periodic and  $U_{\perp}$  is constant in space. With this force, we have  $\mathbf{U}_{\perp}^{\text{eff}} = U_{\perp} \mathbf{e}_y \langle \rho_0 \rangle = U_{\perp} \mathbf{e}_y$ . That is, the particles have a constant speed of translation in  $y$ . This motion, however, has no influence on the transport in the  $x$  direction, as expected.

#### B. Periodic orienting fields

In an external orienting field without geometric confinement, the active particle acquires an angular velocity  $\boldsymbol{\omega}$ , which we assume to be spatially periodic and depends on the particle orientation  $\mathbf{q}$ , i.e.,  $\boldsymbol{\omega} = \boldsymbol{\omega}(\mathbf{x}, \mathbf{q})$ . In the Smoluchowski equation, the rotational flux is written as  $\mathbf{j}_R = \boldsymbol{\omega}(\mathbf{x}) P - D_R \nabla_R P$ . For simplicity, we consider  $\boldsymbol{\omega} = \omega_0 \mathbf{q} \times \hat{\mathbf{H}}$ , where  $\hat{\mathbf{H}}$  is a unit vector in the field direction and  $\omega_0$  is the amplitude.<sup>37,70,71</sup> To achieve a spatially periodic  $\boldsymbol{\omega}$ , one may take the amplitude  $\omega_0$  to be spatially periodic, while  $\hat{\mathbf{H}}$  is constant.

We note that other forms of  $\omega$  may be considered depending on the context.<sup>37,71,72</sup>

Following Secs. II and III A, it is straightforward to obtain the average field equation as

$$\frac{\partial g}{\partial t} + \nabla \cdot (U_s \mathbf{q}g - D_T \nabla g) + \nabla_R \cdot (\omega_0 \mathbf{q} \times \hat{\mathbf{H}}g - D_R \nabla_R g) = 0. \quad (57)$$

The polar order of  $g$  (recall that  $\mathbf{m}_0 = \int_S g \mathbf{q} d\mathbf{q}$ ) satisfies the equation

$$\begin{aligned} \frac{\partial \mathbf{m}_0}{\partial t} + \nabla \cdot \left[ U_s \left( \mathbf{Q}_0 + \frac{\rho_0 \mathbf{I}}{d} \right) - D_T \nabla \mathbf{m}_0 \right] \\ + (d-1) D_R \mathbf{m}_0 + \omega_0 \left( \mathbf{Q}_0 \cdot \hat{\mathbf{H}} - \frac{d-1}{d} \rho_0 \hat{\mathbf{H}} \right) = \mathbf{0}. \end{aligned} \quad (58)$$

Averaging this equation over the unit cell, we obtain

$$\frac{\partial \langle \mathbf{m}_0 \rangle}{\partial t} + (d-1) D_R \langle \mathbf{m}_0 \rangle + \left( \omega_0 \left( \mathbf{Q}_0 \cdot \hat{\mathbf{H}} - \frac{d-1}{d} \rho_0 \hat{\mathbf{H}} \right) \right) = \mathbf{0}. \quad (59)$$

Due to the external orienting field, the cell-averaged polar order does not necessarily vanish. As a result, the average drift is given by

$$\mathbf{U}^{\text{eff}} = U_s \langle \mathbf{m}_0 \rangle. \quad (60)$$

In this case, the net polar order is the only contribution to the average drift velocity.

The displacement field is governed by

$$\begin{aligned} \frac{\partial \mathbf{b}}{\partial t} + \nabla \cdot (U_s \mathbf{q} \mathbf{b} - D_T \nabla \mathbf{b}) + \nabla_R \cdot (\omega_0 \mathbf{q} \times \hat{\mathbf{H}} \mathbf{b} - D_R \nabla_R \mathbf{b}) \\ = 2 D_T \nabla g + (\mathbf{U}^{\text{eff}} - U_s \mathbf{q}) g, \end{aligned} \quad (61)$$

and the dispersion tensor is

$$\mathbf{D}^{\text{eff}} = D_T \mathbf{I} - U_s \langle \mathbf{m}_1 \rangle. \quad (62)$$

We note that fluctuation in the polar order gives a contribution to the diffusivity in addition to  $D_T$ . This is the swim diffusivity in the presence of a spatially periodic orienting field. For the case where both the field direction  $\hat{\mathbf{H}}$  and the amplitude  $\omega_0$  are constant, the swim diffusivity has been considered.<sup>37</sup>

### C. Combined effects of fields and channel confinement

We now derive the macrotransport equations with both external fields and channel confinement. The translational flux that enters the Smoluchowski equation (2) can be written as

$$\mathbf{j}_T = U_s \mathbf{q} P + \mathbf{U}^{\text{ext}}(\mathbf{x}) P - D_T \nabla_X P, \quad (63)$$

where we recall that  $\mathbf{U}^{\text{ext}}$  represents the velocity induced by an external field as discussed in Sec. III A. The rotational flux is given by

$$\mathbf{j}_R = \boldsymbol{\omega}(\mathbf{x}, \mathbf{q}) P - D_R \nabla_R P, \quad (64)$$

where the field-induced angular velocity  $\boldsymbol{\omega}$  can depend on both the local position  $\mathbf{x}$  and the orientation  $\mathbf{q}$ . We note that (63) and (64) can be applied to the transport of ABPs in a periodic flow through a

periodic corrugated channel, in which case  $\mathbf{U}^{\text{ext}}$  is the fluid velocity and  $\boldsymbol{\omega}$  is the particle angular velocity (not equal to the vorticity) due to the flow (see Ref. 2).

Following the procedure given in Sec. II, it is straightforward to show that

$$\mathbf{U}^{\text{eff}} = U_s \mathbf{e}_x \cdot \langle \mathbf{m}_0 \rangle + \mathbf{e}_x \cdot \langle \mathbf{U}^{\text{ext}} \rho_0 \rangle - D_T \mathbf{e}_x \cdot \langle \nabla \rho_0 \rangle, \quad (65a)$$

$$D^{\text{eff}} = D_T - U_s \mathbf{e}_x \cdot \langle \mathbf{m}_1 \rangle - \langle U_x^{\text{ext}} \rho_1 \rangle + D_T \mathbf{e}_x \cdot \langle \nabla \rho_1 \rangle. \quad (65b)$$

For a flat channel, the terms involving  $\nabla \rho_0$  and  $\nabla \rho_1$  in the drift and dispersion coefficients vanish. Furthermore, if the external fields are due to a Poiseuille flow, Eq. (65) reduces to those given by Peng and Brady<sup>39</sup> (see also Sec. II C).

The average field is governed by

$$\frac{\partial g}{\partial t} + \nabla \cdot (U_s \mathbf{q} g + \mathbf{U}^{\text{ext}} g - D_T \nabla g) + \nabla_R \cdot (\boldsymbol{\omega} g - D_R \nabla_R g) = 0. \quad (66)$$

At the no-flux boundaries,  $\mathbf{x} \in \partial \Omega_w$ , we have

$$\mathbf{n} \cdot (U_s \mathbf{q} g + \mathbf{U}^{\text{ext}} g - D_T \nabla g) = 0. \quad (67)$$

The normalization and periodic conditions remain the same as those given in Sec. II A. Similarly, one can show that

$$\begin{aligned} \frac{\partial b}{\partial t} + \nabla \cdot (U_s \mathbf{q} b + \mathbf{U}^{\text{ext}} b - D_T \nabla b) + \nabla_R \cdot (\boldsymbol{\omega} b - D_R \nabla_R b) \\ = 2 D_T \frac{\partial g}{\partial x} + (U^{\text{eff}} - U_s q_x - U_x^{\text{ext}}) g \end{aligned} \quad (68)$$

and

$$\mathbf{n} \cdot (U_s \mathbf{q} b + \mathbf{U}^{\text{ext}} b - D_T \nabla b) = \mathbf{n} \cdot \mathbf{e}_x D_T g, \quad \mathbf{x} \in \partial \Omega_w. \quad (69)$$

The normalization and periodic conditions for  $b$  are given in Sec. II B.

### D. Spatially periodic activity landscape

Active particles in an activity landscape are shown to exhibit density and polarization patterns.<sup>73–80</sup> Tuning the spatial-temporal variation of the swim speed of active particles may allow one to control the system behavior.<sup>81–83</sup> In the absence of channel confinement, we now consider the case in which the active particles are subject to a one-dimensional unbounded and spatially periodic activity landscape. That is, the scalar swim speed is a function of  $x$  with a periodicity of  $L$ ,  $U_s(x+L) = U_s(x)$ .

In the 1D activity landscape, one can show that at long times, the effective transport coefficients in the  $x$  direction are

$$\mathbf{U}^{\text{eff}} = \mathbf{e}_x \cdot \langle U_s \mathbf{m}_0 \rangle \quad \text{and} \quad D^{\text{eff}} = D_T - \mathbf{e}_x \cdot \langle U_s \mathbf{m}_1 \rangle, \quad (70)$$

where the unit cell is  $\Omega = \{x | 0 \leq x \leq L\}$  and the cell-averaging is  $\langle \cdot \rangle = (1/L) \int_0^L (\cdot) dx$ . The average field is governed by

$$\frac{\partial g}{\partial t} + \frac{\partial}{\partial x} \left( U_s q_x g - D_T \frac{\partial g}{\partial x} \right) - D_R \nabla_R^2 g = 0, \quad (71)$$

where  $g$  is spatially periodic and satisfies the normalization  $\langle n_0 \rangle = 1$ , with  $n_0 = \int_S g d\mathbf{q}$ . The displacement field is governed by

$$\frac{\partial b}{\partial t} + \frac{\partial}{\partial x} \left( U_s q_x b - D_T \frac{\partial b}{\partial x} \right) - D_R \nabla_R^2 b = \left( U^{\text{eff}} - U_s q_x \right) g + 2D_T \frac{\partial g}{\partial x}, \quad (72)$$

where  $\langle \int_S b d\mathbf{q} \rangle = 0$ .

We note that the term  $-\mathbf{e}_x \cdot \langle U_s \mathbf{m}_1 \rangle$  in (70) is the swim diffusivity in an activity landscape. For ABPs with a constant speed, at long times,  $g$  and  $b$  are spatially invariant. Supposing that the orientation space is in 2D, we then have  $g = 1/(2\pi)$  and  $b = -\ell/(2\pi)\cos\theta$ , where we have taken  $\mathbf{q} = \cos\theta\mathbf{e}_x + \sin\theta\mathbf{e}_y$ . From this, we obtain  $D^{\text{eff}} = D_T + U_s \ell/2 = D_T + U_s^2 \tau_R/2$ , which is the long-time diffusivity of an ABP in unbounded 2D space with a constant speed  $U_s$ . We further note that the macrotransport equations in a doubly or triply periodic activity landscape can be similarly obtained.

#### IV. ASYMPTOTIC ANALYSIS

##### A. Weak swimming

For convenience, we scale lengths by the spatial periodicity  $L$  of the channel and time by the diffusive timescale  $\tau_D = L^2/D_T$ . At steady state, the non-dimensional equation for  $g$  is

$$\nabla \cdot (Pe \mathbf{q} g - \nabla g) - \gamma^2 \nabla_R^2 g = 0, \quad (73)$$

where we have defined the swimming Péclet number,

$$Pe = \frac{U_s L}{D_T}, \quad (74)$$

and

$$\gamma = \sqrt{D_R \tau_D}. \quad (75)$$

To study the first effect of swimming on the macrotransport, we pose a regular expansion for  $g$  in the weak-swimming limit characterized by  $Pe \ll 1$ ,

$$g = g^{(0)} + Pe g^{(1)} + Pe^2 g^{(2)} + \dots \quad (76)$$

Similarly, the orientational moments are written as

$$\rho_0 = \rho_0^{(0)} + Pe \rho_0^{(1)} + Pe^2 \rho_0^{(2)} + \dots, \quad (77a)$$

$$\mathbf{m}_0 = \mathbf{m}_0^{(0)} + Pe \mathbf{m}_0^{(1)} + Pe^2 \mathbf{m}_0^{(2)} + \dots. \quad (77b)$$

At  $O(1)$ , the swimming motion is absent, and the particles exhibit (passive) Brownian motion. The solution is readily obtained to be

$$g^{(0)}(\mathbf{x}, \mathbf{q}) = \frac{1}{|\mathcal{S}|}, \quad (78)$$

where  $\mathcal{S}^d$  is the total “volume” of the orientation space. As expected, for Brownian particles, the density is uniform,  $\rho_0^{(0)} = 1$ , and the

average drift is zero.

At  $O(Pe)$ , one can show that the density  $\rho_0^{(1)} = 0$ , and the polar order is governed by

$$-\nabla^2 \mathbf{m}_0^{(1)} + (d-1)\gamma^2 \mathbf{m}_0^{(1)} = \mathbf{0}, \quad (79a)$$

$$\mathbf{n} \cdot \nabla \mathbf{m}_0^{(1)} = \frac{1}{d} \mathbf{n}, \quad \mathbf{x} \in \partial \Omega_w. \quad (79b)$$

The periodic conditions also apply for  $\mathbf{m}_0^{(1)}$ . Because the density at  $O(Pe)$  vanishes, the  $O(Pe)$  average drift is zero.

The first non-zero average drift can be obtained at  $O(Pe^2)$ ; the number density is given by

$$\nabla^2 \rho_0^{(2)} = \nabla \cdot \mathbf{m}_0^{(1)}, \quad (80a)$$

$$\mathbf{n} \cdot \nabla \rho_0^{(2)} = \mathbf{n} \cdot \mathbf{m}_0^{(1)}, \quad \mathbf{x} \in \partial \Omega_w. \quad (80b)$$

From (31), we have the dimensional drift

$$U^{\text{eff}} = -Pe^2 \frac{D_T}{|\Omega|} \mathbf{e}_x \cdot \int_{\partial \Omega_i \cup \partial \Omega_b} \mathbf{n} \rho_0^{(2)} dS + o(Pe^2). \quad (81)$$

To calculate the leading-order drift using the preceding equation, one needs to specify the channel geometry. Nevertheless, a straightforward scaling analysis of (81) reveals the general behavior that  $U^{\text{eff}}/U_s \sim Pe$  as  $Pe \rightarrow 0$  for a fixed  $\gamma$  (provided that the channel is not fore-aft symmetric). This is an important result of this section: the average drift scaled by the swim speed grows linearly in the weak-swimming limit. Alternatively, scaling the drift by the diffusive speed  $D_T/L$ , we have  $U^{\text{eff}}/(D_T/L) \sim Pe^2$ . One may interpret the ratio  $U^{\text{eff}}/U_s$  as a rectification efficiency since at most one could align all particles in the same direction via external means and obtain the theoretical maximum of unity:  $U^{\text{eff}}/U_s = 1$  when  $g(\mathbf{x}, \mathbf{q}, t) = \rho_0(\mathbf{x}, t) \delta(\mathbf{q} - \mathbf{e}_x)$ , where  $\delta$  is the Dirac delta function. Under channel confinement, particles at the wall tend to point into the wall and their orientations are not strongly aligned with  $\mathbf{e}_x$ . As a result, the rectification efficiency in periodic channels is often small.

Next, we consider the displacement field and the resulting dispersion coefficient in the weak swimming limit. The non-dimensional displacement field equation at long times is given by

$$\nabla \cdot (Pe \mathbf{q} b - \nabla b) - \gamma^2 \nabla_R^2 b = 2 \frac{\partial g}{\partial x} + \left( U^{\text{eff}} - Pe q_x \right) g, \quad (82)$$

where  $U^{\text{eff}}$  is non-dimensionalized by the diffusive speed  $L/D_T$  and  $b$  is non-dimensionalized by  $L$ . Similar to (76) and (77), we may write

$$b = b^{(0)} + Pe b^{(1)} + Pe^2 b^{(2)} + \dots, \quad (83a)$$

$$\rho_1 = \rho_1^{(0)} + Pe \rho_1^{(1)} + Pe^2 \rho_1^{(2)} + \dots, \quad (83b)$$

$$\mathbf{m}_1 = \mathbf{m}_1^{(0)} + Pe \mathbf{m}_1^{(1)} + Pe^2 \mathbf{m}_1^{(2)} + \dots. \quad (83c)$$

At  $O(1)$ , recall that the particles are passive, and we obtain

$$-\nabla^2 b^{(0)} - \gamma^2 \nabla_R^2 b^{(0)} = 2 \frac{\partial g^{(0)}}{\partial x} = 0, \quad (84a)$$

$$-\mathbf{n} \cdot \nabla b^{(0)} = \mathbf{n} \cdot \mathbf{e}_x g^{(0)}, \quad \mathbf{x} \in \partial\Omega_w. \quad (84b)$$

In the absence of swimming, the orientational distribution is uniform, and we have  $b^{(0)} = \rho_1^{(0)}/|\mathbb{S}|$ . This means that the polar order vanishes,  $\mathbf{m}_1^{(0)} = \mathbf{0}$ , and we only need to consider the number density. From (84), we have

$$-\nabla^2 \rho_1^{(0)} = 0, \quad (85a)$$

$$-\mathbf{n} \cdot \nabla \rho_1^{(0)} = \mathbf{n} \cdot \mathbf{e}_x, \quad \mathbf{x} \in \partial\Omega_w. \quad (85b)$$

The preceding equations govern the fluctuations in the density field of passive particles, which affects the dispersion coefficient. Equation (85) is the same as (43), which were obtained by setting the swim speed to zero. The density field  $\rho_1^{(0)}$  contributes to the dispersion coefficient [see (44)]. This contribution is a purely passive result.

It follows from (36) that the net density must vanish,

$$\int_{\Omega} \rho_1^{(0)} d\mathbf{x} = 0. \quad (86)$$

At  $O(Pe)$ , the  $b$  field is governed by

$$\nabla \cdot (\mathbf{q} b^{(0)} - \nabla b^{(1)}) - \gamma^2 \nabla_R^2 b^{(1)} = 2 \frac{\partial g^{(1)}}{\partial x} - q_x g^{(0)}, \quad (87a)$$

$$\mathbf{n} \cdot (\mathbf{q} b^{(0)} - \nabla b^{(1)}) = \mathbf{n} \cdot \mathbf{e}_x g^{(1)}, \quad \mathbf{x} \in \partial\Omega_w. \quad (87b)$$

Recalling that  $\rho_0^{(1)} = 0$  and  $b^{(0)}$  does not depend on  $\mathbf{q}$ , we conclude that the density at  $O(Pe)$ ,  $\rho_1^{(1)} = \int b^{(1)} d\mathbf{q} = 0$ . The polar order, however, does not vanish; it is governed by

$$\nabla \cdot \left( \frac{\mathbf{I}}{d} \rho_1^{(0)} - \nabla \mathbf{m}_1^{(1)} \right) + (d-1) \gamma^2 \mathbf{m}_1^{(1)} = 2 \frac{\partial \mathbf{m}_0^{(1)}}{\partial x} - \frac{\mathbf{e}_x}{d}, \quad (88a)$$

$$\mathbf{n} \cdot \left( \frac{\mathbf{I}}{d} \rho_1^{(0)} - \nabla \mathbf{m}_1^{(1)} \right) = \mathbf{n} \cdot \mathbf{e}_x \mathbf{m}_0^{(1)}, \quad \mathbf{x} \in \partial\Omega_w. \quad (88b)$$

Because the density at  $O(Pe)$  vanishes, there is no active contribution to the dispersion at this order [see the last term in (42)].

To seek the first active contribution to the dispersion coefficient, we have to consider the density field at  $O(Pe^2)$ . Following the expansion procedure, one can show that  $\rho_1^{(2)}$  satisfies

$$\nabla \cdot (\mathbf{m}_1^{(1)} - \nabla \rho_1^{(2)}) = 2 \frac{\partial \rho_0^{(2)}}{\partial x} + U^{(2)} - \mathbf{e}_x \cdot \mathbf{m}_0^{(1)}, \quad (89a)$$

$$\mathbf{n} \cdot (\mathbf{m}_1^{(1)} - \nabla \rho_1^{(2)}) = \mathbf{n} \cdot \mathbf{e}_x \rho_0^{(2)}, \quad \mathbf{x} \in \partial\Omega_w. \quad (89b)$$

Taken together, we obtain the dispersion coefficient as

$$\begin{aligned} \frac{D^{\text{eff}}}{D_T} &= \frac{D_{\text{passive}}^{\text{eff}}}{D_T} + \frac{D_0^{\text{swim}}}{D_T} \left( 1 - d \left( \frac{\partial m_{0,x}^{(1)}}{\partial x} \right) \right) \\ &\quad + Pe^2 \left( \frac{\partial \rho_1^{(2)}}{\partial x} \right) + o(Pe^2), \end{aligned} \quad (90)$$

where we remark that  $x$ ,  $\rho_1^{(2)}$ , and  $\mathbf{m}_0^{(1)}$  are non-dimensional. Equation (90) is the second key result of this section. In the absence of activity ( $Pe \equiv 0$ ), the longitudinal dispersion coefficient is given by the purely passive result of (44). Noting that  $D_0^{\text{swim}}/D_T = Pe^2/[\gamma^2 d(d-1)]$ , we conclude that the first active contribution to  $D^{\text{eff}}/D_T$  is  $O(Pe^2)$ . Note that in asymmetric channels, the undisturbed swim diffusivity  $D_0^{\text{eff}}/D_T$  is corrected by the average  $x$  gradient of the polar order  $m_{0,x}^{(1)}$ . Furthermore, the active density fluctuation also contributes to the dispersion, as given by the first term on the second line of (90). We note that the passive density fluctuation is accounted for in  $D_{\text{passive}}^{\text{eff}}$ .

## B. Nearly flat channels

In this section, we consider nearly flat channels defined by

$$y_{\pm} = W[\pm 1 + \varepsilon w_{\pm}(x)], \quad (91)$$

where  $W$  is the half-width of the unperturbed flat channel. The channel modulations are assumed to be small, i.e.,  $\varepsilon w_{\pm}(x) \ll 1$ . Periodicity requires that  $w_{\pm}(x+L) = w_{\pm}(x)$ . In the small-modulation limit, we seek an asymptotic solution via

$$g = g^{(0)} + \varepsilon g^{(1)} + \dots, \quad (92a)$$

$$b = b^{(0)} + \varepsilon b^{(1)} + \dots. \quad (92b)$$

The unit normal vector at  $y = y_+$  can be expanded as

$$\mathbf{n}|_{y_+} = \mathbf{e}_y + \varepsilon \mathbf{n}^{(1)} + O(\varepsilon^2), \quad (93)$$

where  $\mathbf{n}^{(1)} = -Ww'_+(x)\mathbf{e}_x$ . Similarly, the unit outward normal to the bottom wall  $\mathbf{n}|_{y_-} = -\mathbf{e}_y + \varepsilon Ww'_- \mathbf{e}_x + O(\varepsilon^2)$ .

To study the first effect of small-amplitude modulations, we recast the problem onto the unperturbed domain. From (31), one can show that the leading-order contribution to the average drift is  $O(\varepsilon^2)$ ,  $U^{\text{eff}} = \varepsilon^2 U^{(2)} + \dots$ , where

$$U^{(2)} = \frac{D_T}{2L} \int_0^L \left( w'_+ \rho_0^{(1)} \Big|_W - w'_- \rho_0^{(1)} \Big|_{-W} \right) dx. \quad (94)$$

In the above,  $(\cdot)|_{y^*}$  is a shorthand for evaluating the expression at  $y = y^*$ . Similarly, the effective dispersion coefficient admits the expansion  $D^{\text{eff}} = D_0^{\text{eff}} + \varepsilon^2 D^{(2)} + \dots$ , where

$$\begin{aligned} D^{(2)} &= \frac{U_s \delta^2 W}{d-1} \int_0^L \left( w'_+ m_{0,x}^{(1)} \Big|_W - w'_- m_{0,x}^{(1)} \Big|_{-W} \right) dx \\ &\quad - D_T W \int_0^L \left( w'_+ \rho_1^{(1)} \Big|_W - w'_- \rho_1^{(1)} \Big|_{-W} \right) dx. \end{aligned} \quad (95)$$

It is clear that for a flat channel,  $\varepsilon \equiv 0$ , the average drift vanishes and the effective dispersion coefficient is  $D_0^{\text{eff}} = D_T + D_0^{\text{swim}}$ .

To calculate  $U^{(2)}$  and  $D^{(2)}$ , we need the fields  $g^{(1)}$  and  $b^{(1)}$  defined in (92). We first expand  $g$  at  $y = y_+$  about the unperturbed boundary  $y = W$  in a Taylor series, which gives

$$g|_{y_+} = g|_W + \frac{\partial g}{\partial y} \Big|_W \varepsilon w_+ W + \dots. \quad (96)$$

Combining (92a) and (96), we have

$$g|_{y_+} = g^{(0)} \Big|_W + \varepsilon \left( g^{(1)} \Big|_W + \frac{\partial g^{(0)}}{\partial y} \Big|_W w_+ W \right) + O(\varepsilon^2). \quad (97)$$

For the bottom wall,  $y = y_-$ , a similar expansion can be written. At  $O(\varepsilon^p)$ ,  $p = 0, 1, 2, \dots$ , Eq. (23) remains unchanged, which gives

$$\nabla \cdot \left( U_s q g^{(p)} - D_T \nabla g^{(p)} \right) - D_R \nabla_R^2 g^{(p)} = 0. \quad (98)$$

At  $O(1)$ , the channel is flat, and the no-flux condition becomes

$$U_s q y g^{(0)} - D_T \frac{\partial g^{(0)}}{\partial y} = 0, \quad y = \pm W. \quad (99)$$

Note that the boundary condition is now imposed at the unperturbed flat walls, which is the purpose of the domain perturbation analysis. Equations (98) and (99) specify the dynamics of ABPs in a flat channel;  $g^{(0)}$  is invariant in  $x$ .

At  $O(\varepsilon)$ , the no-flux condition is

$$\begin{aligned} U_s q_y g^{(1)} - D_T \left( \frac{\partial g^{(1)}}{\partial y} + w_\pm W \frac{\partial^2 g^{(0)}}{\partial y^2} \right) \\ = w'_\pm W \left( U_s q_x g^{(0)} - D_T \frac{\partial g^{(0)}}{\partial x} \right), \quad y = \pm W, \end{aligned} \quad (100)$$

where the last term vanishes because  $\partial g^{(0)}/\partial x = 0$ . Following the above procedure, one may obtain the governing equations for  $b^{(0)}$  and  $b^{(1)}$ , from which the density and polar order of the displacement field can be calculated.

## V. NUMERICAL EXAMPLES

To provide a direct numerical validation of our macrotransport equations, we compare the macrotransport coefficients obtained from the macrotransport theory with those obtained from BD simulations. We describe below the rectified transport and long-time dispersion dynamics of ABPs in asymmetric confinement. The mean and displacement equations are solved using a standard finite element method (FEM) implemented in FreeFem++.<sup>34</sup> In BD simulations, the corresponding Langevin equations of motion of an ABP are integrated in time using a standard Euler–Maruyama scheme. The drift coefficient is obtained by fitting the slope of the mean-displacement curve at long times. The implementation details of FEM and BD are presented in the supplementary material.

### A. An asymmetric channel

For an ABP in an asymmetric channel, the non-dimensional average and displacement equations are, respectively, (73) and (82). Once the macrotransport equations are solved, we calculate the average drift and effective dispersion coefficient using (20a) and (20b). In Fig. 2(a), we plot the average drift scaled by the swim speed as a function of the swimming Péclet number ( $Pe$ ). The dimensionless drift increases with increasing  $Pe$  (or swim speed) before it saturates at large  $Pe$ . As derived in Sec. IV A using an asymptotic analysis, we have  $U^{eff}/U_s \sim Pe$  for slow swim speeds. Such a linear scaling has been inferred from fitting BD simulation data.<sup>17</sup>

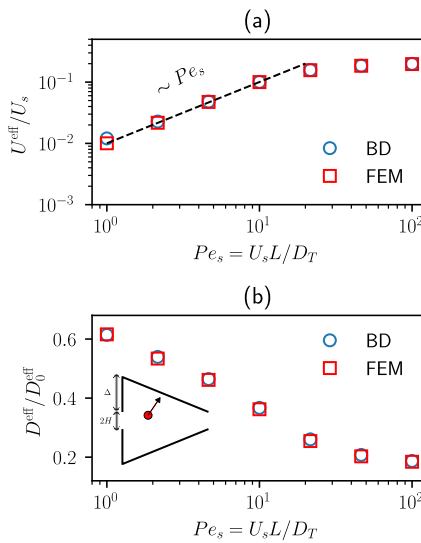


**FIG. 2.** (a) The dimensionless average drift  $U^{eff}/U_s$  as a function of the swimming Péclet number ( $Pe_s = U_s L / D_T$ ). (b) The dimensionless effective dispersion coefficient  $D^{eff}/D_0^{eff}$  as a function of the swimming Péclet number ( $Pe_s = U_s L / D_T$ ). For both (a) and (b),  $y = 1$ , and the channel unit cell is shown in the inset of (b). The geometry of the channel is characterized by  $H/L = 0.1$  and  $\Delta/L = 0.4$ , where  $L$  is the (horizontal) length of the unit cell. No external forces or fields are considered. Square symbols denote theoretical results obtained from solving the macrotransport equations using a standard finite element method (FEM). Circles are results from BD simulations. The dashed line in (a) shows a linear dependence of  $U^{eff}/U_s$  on  $Pe_s$  (see Sec. IV A).

In Fig. 2(b), we plot the longitudinal dispersion coefficient scaled by  $D_0^{eff}$  (recall that  $D_0^{eff} = D_T + D_0^{swim}$ ) as a function of  $Pe$ . As the swim speed increases, the reduction in dispersion is more pronounced because the effective run length is reduced as particles become more confined ( $\ell/W = U_s \tau_R/W \gg 1$ , where  $W$  is the characteristic width of the channel). We note that the confinement-induced hindrance in effective diffusion has been observed.<sup>19,85</sup> For both the drift and dispersion coefficient, good agreement between the macrotransport theory (squares) and BD (circles) simulations is observed.

In Fig. 3, we show the number density distribution of the average field for (a)  $Pe = 1$  and (b)  $Pe = 10$ . The number density field is obtained by taking the zeroth moment of the FEM solution of  $g$ . That is, we calculate the integral ( $\rho_0 = \int_S g d\mathbf{q}$ ) using the trapezoidal rule. For low activity (e.g.,  $Pe = 1$ ), we see that the density gradient is very weak. When activity is high (e.g.,  $Pe = 10$ ), the boundary accumulation of ABPs can be seen clearly from the steep density gradients near the top and bottom corners. As shown by our theory, the net diffusive flux gives the average drift. From Fig. 3(b), we see that the density is higher on the left side compared with that on the right. Therefore, the net motion is toward the right, i.e.,  $U^{eff} > 0$ .

### B. An asymmetric substrate potential

Consider an ABP subject to an asymmetric substrate potential given by  $V(x) = V_0[\sin(2\pi x/L) + \sin(4\pi x/L)/4]$  in two dimensions.<sup>24</sup> The force exerted on the particle due to the potential is  $\mathbf{F} = -\partial V/(\partial x)\mathbf{e}_x$ . Note that the potential has a periodicity of  $L$  and

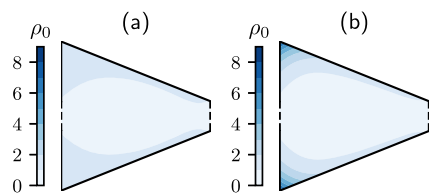


**FIG. 3.** The number density distribution ( $\rho_0$ ) in the unit cell for (a)  $Pe = 1$  and (b)  $Pe = 10$  obtained from FEM. For both panels, we have  $\gamma = 1$ . The geometric parameters of the channel are given in Fig. 2. The channel openings on the left and right are shown by dashed lines, while the no-flux walls are shown by solid lines.

the force biases the particles toward the negative  $x$  direction. Besides  $Pe$  and  $\gamma$  introduced in Sec. IV A, the system is also governed by a Péclet number of the external potential, which is defined as  $Pe_V = V_0\pi/(\zeta D_T)$ .

We show the macrotransport coefficients along the  $x$  direction in Fig. 4. The dimensionless average drift as a function of  $Pe$  is plotted in Fig. 4(a). Because the drift is negative, the quantity  $-U^{\text{eff}}/U_s$  is plotted. In Fig. 4(b), we plot the dimensionless dispersion coefficient ( $D^{\text{eff}}/D_T$ ) as a function of  $Pe$ . Good agreement between the theory (FEM) and BD simulations is observed. Different from a hard wall that can exert a force as large as necessary to prevent a particle from moving beyond the no-flux boundary, a substrate potential is soft. When the swim force ( $\zeta U_s$ ) exceeds the potential force, the effect of the potential becomes weak. For a fixed  $Pe_V$ , we therefore observe that the net ratchet flux vanishes and the effective diffusivity

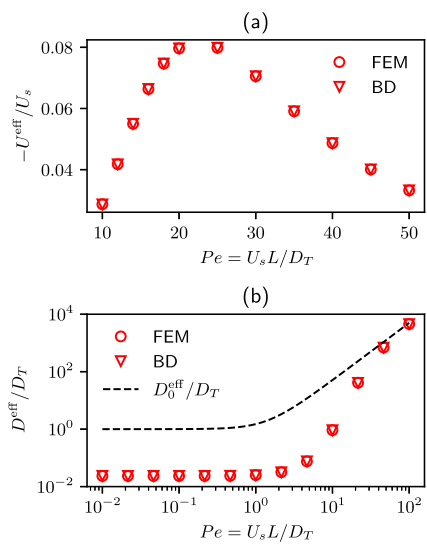


**FIG. 4.** Macrotransport coefficients of ABPs in a one-dimensional periodic substrate potential. (a) The dimensionless average drift  $-U^{\text{eff}}/U_s$  as a function of the swimming Péclet number ( $Pe_s = U_s L/D_T$ ). We note that  $U^{\text{eff}}$  is negative. (b) The dimensionless effective dispersion coefficient  $D^{\text{eff}}/D_T$  as a function of the swimming Péclet number ( $Pe_s = U_s L/D_T$ ). For both (a) and (b),  $\gamma = 1$  and  $Pe_V = 10$ . Circle symbols denote theoretical results obtained from solving the macrotransport equations using FEM. Triangles are results from BD simulations. The free-space result is shown by the dashed line.

approaches  $D_0^{\text{eff}}$  as  $Pe \rightarrow \infty$ . As shown in Fig. 4(a), the dimensionless average drift varies non-monotonically as a function of  $Pe$ . The maximum rectification efficiency (defined as  $-U^{\text{eff}}/U_s$ ) is achieved when the swim force is comparable with the force due to the potential. The force due to the substrate potential suppresses the effective dispersion. As a result, we see in Fig. 4(b) that  $D^{\text{eff}}$  is lower than  $D_0^{\text{eff}}$  for finite  $Pe$ . In the large- $Pe$  limit,  $D^{\text{eff}}$  approaches that of the free-space value since the substrate force becomes sub-dominant.

## VI. DISCUSSION

In this paper, we have developed a macrotransport theory for active Brownian particles in spatially periodic domains. By decomposing the position vector into the cell vector and a local position vector, we derived a pair of macrotransport equations that characterize the long-time transport dynamics of active particles. Our macrotransport theory can be treated as a generalized Taylor dispersion theory (GTDT) for periodic geometries. In the language of GTDT, the cell index is the global space, while the local position vector and the orientation vector constitute the local space. Leveraging this generic framework, we derived macrotransport equations for active particles in corrugated channels, spatially periodic external fields, and activity landscapes. Under geometric confinement, while the focus was on corrugated periodic channels, the theoretical model can readily accommodate the macrotransport processes of active particles in periodic porous media.<sup>60,65,85,86</sup>

For active particles confined in a corrugated periodic channel in the absence of external forces and fields, it is known that the active Brownian motion under a no-flux boundary condition can be rectified, provided that the unit cell of the channel is fore-aft asymmetric. Complementing previous works on BD simulations and experiments, our approach provides a statistical mechanical description of the rectification mechanism. Regardless of activity, the average drift or rectified flux is given by the net diffusive flux along the channel. For passive Brownian motion, the density is homogeneous, and no net flux is generated. In the case of active particles, their activity coupled with confinement can support a non-zero density gradient. Ultimately, such a density gradient leads to rectified transport. This autonomous rectification reflects the non-equilibrium nature of active systems. In addition to the average drift, the macrotransport theory allows us to characterize the longitudinal dispersion coefficient of active particles. While different boundary conditions may be incorporated in the GTDT, in this work, we focused on the case of a no-flux boundary condition. For the cases of periodic potentials or fields in the absence of channel confinement, only periodic conditions due to the geometry are needed.

In modeling the effective longitudinal dynamics of (passive) Brownian motion under spatially varying confinement, such as a corrugated channel, the Fick-Jacobs (FJ) theory has been widely adopted.<sup>87–93</sup> The FJ theory reduces the problem of diffusion in two- or three-dimensional channels to an effective one-dimensional (1D) problem along the channel axis. This is done by averaging over the cross section of the channel, which often relies on the assumption that the cross section varies slowly. In doing so, the spatial variation of the channel is incorporated into an effective diffusion coefficient that depends on the channel geometry. Often, the dependence of the diffusion coefficient in the 1D equation on the channel geometry is

defined heuristically.<sup>89,91</sup> Recently, the FJ theory has been extended to accommodate active Brownian motion<sup>85</sup> by treating active particles as (passive) Brownian particles at a higher effective temperature. Not surprisingly, the FJ theory deviates from the BD simulation results when active particles are sufficiently confined. Despite the discrepancy, the simplicity of FJ theory allows one to obtain a quick estimate of the dispersion behavior. In contrast, we emphasize that our macrotransport theory does not restrict the geometry of the channel unit cell. Said differently, the macrotransport theory works equally well regardless of the degree of confinement that the active particles experience. As such, it does not impose a restriction on the variation of the channel walls or on the run length (or activity) of the active particles. Because the macrotransport equations depend on the full position-orientation space coordinates (unlike the 1D equation in FJ theory), their application often requires numerical solutions of partial differential equations, as demonstrated in Fig. 2.

To develop the macrotransport theory, several simplifying assumptions have been made. The governing equations are written for a single point-sized particle in the absence of particle-particle and particle-wall hydrodynamic interactions. Even for single particle dynamics, finite-size effects may become important if the width of the channel is comparable to the size of the particle. In this case, one may still employ the single-particle Smoluchowski equation, but the appropriate hydrodynamic resistance tensors need to be considered. For active particle systems with finite densities, interactions among particles—whether hydrodynamic or otherwise—may play a role in dictating the macrotransport dynamics. In principle, one can make use of the multi-particle Smoluchowski equation to develop a statistical mechanical description.<sup>94</sup> However, the high-dimensionality of such equations poses a computational challenge. As such, particle-based simulation methods may be more convenient for investigating the transport processes of semi-dilute and dense systems. In the case of passive-active mixtures, the macrotransport dynamics under asymmetric confinement become more intricate.<sup>17,95–98</sup> Recent work suggests that depending on the channel and particle geometry, the drift of the mixture can be in either direction of the channel.<sup>98</sup>

In this work, the asymmetric confining boundaries (e.g., corrugated channel) are not allowed to move. To obey momentum balance, active particles subject to a no-flux boundary condition exhibit a rectified flux. In the case of an asymmetric passive object immersed in a bath of active particles, the object itself can exhibit directed linear motion.<sup>22,99–101</sup> Similarly, a gear with asymmetric teeth immersed in an active bath can exhibit directed rotational motion.<sup>12–16</sup> Our work provides a mathematical foundation to develop statistical mechanical theories to characterize the transport mechanics of immersed objects in an active bath. Theoretical models can be useful in identifying limits in the extent of useful work that can be extracted from the active Brownian motion of the bath. In addition, it will be useful for the development of design principles for activity-induced transport.<sup>53,102</sup>

## SUPPLEMENTARY MATERIAL

In the [supplementary material](#), we provide details of mathematical derivations, FEM, and BD simulations.

## AUTHOR DECLARATIONS

### Conflict of Interest

The author has no conflicts to disclose.

### Author Contributions

**Zhiwei Peng:** Conceptualization (lead); Formal analysis (lead); Investigation (lead); Methodology (lead); Software (lead); Writing – original draft (lead); Writing – review & editing (lead).

## DATA AVAILABILITY

The data that support the findings of this study are available within the article.

## REFERENCES

- N. Figueroa-Morales, A. Rivera, R. Soto, A. Lindner, E. Altshuler, and É. Clément, “E. coli ‘super-contaminates’ narrow ducts fostered by broad run-time distribution,” *Sci. Adv.* **6**, eaay0155 (2020).
- T. Zhou, X. Wan, D. Z. Huang, Z. Li, Z. Peng, A. Anandkumar, J. F. Brady, P. W. Sternberg, and C. Daraio, “AI-aided geometric design of anti-infection catheters,” *Sci. Adv.* **10**, eadj1741 (2024).
- W. Gao and J. Wang, “Synthetic micro/nanomotors in drug delivery,” *Nanoscale* **6**, 10486–10494 (2014).
- H. Xu, M. Medina-Sánchez, V. Magdanz, L. Schwarz, F. Hebenstreit, and O. G. Schmidt, “Sperm-hybrid micromotor for targeted drug delivery,” *ACS Nano* **12**, 327–337 (2018).
- B. E.-F. de Avila, P. Angsantikul, J. Li, M. Angel Lopez-Ramirez, D. E. Ramirez-Herrera, S. Thamphiwatana, C. Chen, J. Delezuk, R. Samakapiruk, V. Ramez *et al.*, “Micromotor-enabled active drug delivery for in vivo treatment of stomach infection,” *Nat. Commun.* **8**, 272 (2017).
- P. Romanczuk, M. Bär, W. Ebeling, B. Lindner, and L. Schimansky-Geier, “Active Brownian particles: From individual to collective stochastic dynamics,” *Eur. Phys. J.: Spec. Top.* **202**, 1–162 (2012).
- C. Bechinger, R. Di Leonardo, H. Löwen, C. Reichhardt, G. Volpe, and G. Volpe, “Active particles in complex and crowded environments,” *Rev. Mod. Phys.* **88**, 045006 (2016).
- Y. Yan and J. F. Brady, “The force on a boundary in active matter,” *J. Fluid Mech.* **785**, R1 (2015).
- F. Smallenburg and H. Löwen, “Swim pressure on walls with curves and corners,” *Phys. Rev. E* **92**, 032304 (2015).
- W. Yan and J. F. Brady, “The curved kinetic boundary layer of active matter,” *Soft Matter* **14**, 279–290 (2018).
- Y. Hiratsuka, M. Miyata, T. Tada, and T. Q. Uyeda, “A microrotary motor powered by bacteria,” *Proc. Natl. Acad. Sci. U. S. A.* **103**, 13618–13623 (2006).
- L. Angelani, R. Di Leonardo, and G. Ruocco, “Self-starting micromotors in a bacterial bath,” *Phys. Rev. Lett.* **102**, 048104 (2009).
- A. Sokolov, M. M. Apodaca, B. A. Grzybowski, and I. S. Aranson, “Swimming bacteria power microscopic gears,” *Proc. Natl. Acad. Sci. U. S. A.* **107**, 969–974 (2010).
- R. Di Leonardo, L. Angelani, D. Dell’Arciprete, G. Ruocco, V. Iebba, S. Schippa, M. P. Conte, F. Mecarini, F. De Angelis, and E. Di Fabrizio, “Bacterial ratchet motors,” *Proc. Natl. Acad. Sci. U. S. A.* **107**, 9541–9545 (2010).
- M. J. Y. Jerez, M. A. Bonachita, and M. N. P. Confesor, “Dynamics of a ratchet gear powered by an active granular bath,” *Phys. Rev. E* **101**, 022604 (2020).
- G.-h. Xu and B.-q. Ai, “Rotation reversal of a ratchet gear powered by active particles,” *Soft Matter* **17**, 7124–7132 (2021).
- P. K. Ghosh, V. R. Misko, F. Marchesoni, and F. Nori, “Self-propelled Janus particles in a ratchet: Numerical simulations,” *Phys. Rev. Lett.* **110**, 268301 (2013).

- <sup>18</sup>B.-q. Ai, Q.-y. Chen, Y.-f. He, F.-g. Li, and W.-r. Zhong, "Rectification and diffusion of self-propelled particles in a two-dimensional corrugated channel," *Phys. Rev. E* **88**, 062129 (2013).
- <sup>19</sup>X. Ao, P. K. Ghosh, Y. Li, G. Schmid, P. Hänggi, and F. Marchesoni, "Active Brownian motion in a narrow channel," *Eur. Phys. J.: Spec. Top.* **223**, 3227–3242 (2014).
- <sup>20</sup>P. K. Ghosh, P. Hänggi, F. Marchesoni, and F. Nori, "Giant negative mobility of Janus particles in a corrugated channel," *Phys. Rev. E* **89**, 062115 (2014).
- <sup>21</sup>B.-q. Ai, "Ratchet transport powered by chiral active particles," *Sci. Rep.* **6**, 18740 (2016).
- <sup>22</sup>C. O. Reichhardt and C. Reichhardt, "Ratchet effects in active matter systems," *Annu. Rev. Condens. Matter Phys.* **8**, 51–75 (2017).
- <sup>23</sup>J. A. Drocco, C. J. Olson Reichhardt, and C. Reichhardt, "Bidirectional sorting of flocking particles in the presence of asymmetric barriers," *Phys. Rev. E* **85**, 056102 (2012).
- <sup>24</sup>C. Reichhardt and C. J. O. Reichhardt, "Active matter ratchets with an external drift," *Phys. Rev. E* **88**, 062310 (2013).
- <sup>25</sup>V. Kantsler, J. Dunkel, M. Polin, and R. E. Goldstein, "Ciliary contact interactions dominate surface scattering of swimming eukaryotes," *Proc. Natl. Acad. Sci. U. S. A.* **110**, 1187–1192 (2013).
- <sup>26</sup>M. S. Davies Wykes, X. Zhong, J. Tong, T. Adachi, Y. Liu, L. Ristroph, M. D. Ward, M. J. Shelley, and J. Zhang, "Guiding microscale swimmers using teardrop-shaped posts," *Soft Matter* **13**, 4681–4688 (2017).
- <sup>27</sup>J. Tong and M. J. Shelley, "Directed migration of microscale swimmers by an array of shaped obstacles: Modeling and shape optimization," *SIAM J. Appl. Math.* **78**, 2370–2392 (2018).
- <sup>28</sup>L. Angelani, A. Costanzo, and R. Di Leonardo, "Active ratchets," *Europhys. Lett.* **96**, 68002 (2011).
- <sup>29</sup>B.-Q. Ai and F.-G. Li, "Transport of underdamped active particles in ratchet potentials," *Soft Matter* **13**, 2536–2542 (2017).
- <sup>30</sup>N. Nikola, A. P. Solon, Y. Kafri, M. Kardar, J. Tailleur, and R. Voituriez, "Active particles with soft and curved walls: Equation of state, ratchets, and instabilities," *Phys. Rev. Lett.* **117**, 098001 (2016).
- <sup>31</sup>J. M. Barakat and S. C. Takatori, "Enhanced dispersion in an oscillating array of harmonic traps," *Phys. Rev. E* **107**, 014601 (2023).
- <sup>32</sup>Z. Peng, "Rotational Taylor dispersion in linear flows," *J. Fluid Mech.* **997**, A10 (2024).
- <sup>33</sup>B. Ezhilan and D. Saintillan, "Transport of a dilute active suspension in pressure-driven channel flow," *J. Fluid Mech.* **777**, 482–522 (2015).
- <sup>34</sup>L. N. Trefethen, *Spectral Methods in MATLAB* (SIAM, 2000).
- <sup>35</sup>J. F. Morris and J. F. Brady, "Self-diffusion in sheared suspensions," *J. Fluid Mech.* **312**, 223–252 (1996).
- <sup>36</sup>R. N. Zia and J. F. Brady, "Single-particle motion in colloids: Force-induced diffusion," *J. Fluid Mech.* **658**, 188–210 (2010).
- <sup>37</sup>S. C. Takatori and J. F. Brady, "Swim stress, motion, and deformation of active matter: Effect of an external field," *Soft Matter* **10**, 9433–9445 (2014).
- <sup>38</sup>E. W. Burkholder and J. F. Brady, "Tracer diffusion in active suspensions," *Phys. Rev. E* **95**, 052605 (2017).
- <sup>39</sup>Z. Peng and J. F. Brady, "Upstream swimming and Taylor dispersion of active Brownian particles," *Phys. Rev. Fluids* **5**, 073102 (2020).
- <sup>40</sup>E. Taghizadeh, F. J. Valdés-Parada, and B. D. Wood, "Preasymptotic Taylor dispersion: Evolution from the initial condition," *J. Fluid Mech.* **889**, A5 (2020).
- <sup>41</sup>M. Guan, W. Jiang, B. Wang, L. Zeng, Z. Li, and G. Chen, "Pre-asymptotic dispersion of active particles through a vertical pipe: The origin of hydrodynamic focusing," *J. Fluid Mech.* **962**, A14 (2023).
- <sup>42</sup>The average polar order would not vanish in the presence of external orienting fields.
- <sup>43</sup>W. Yan and J. F. Brady, "The swim force as a body force," *Soft Matter* **11**, 6235–6244 (2015).
- <sup>44</sup>J. F. Brady, "Brownian motion, hydrodynamics, and the osmotic pressure," *J. Chem. Phys.* **98**, 3335–3341 (1993).
- <sup>45</sup>A. D. Maude, "Non-random distribution of bull spermatozoa in a drop of sperm suspension," *Nature* **200**, 381 (1963).
- <sup>46</sup>G. Li and J. X. Tang, "Accumulation of microswimmers near a surface mediated by collision and rotational Brownian motion," *Phys. Rev. Lett.* **103**, 078101 (2009).
- <sup>47</sup>G. Li, J. Bensson, L. Nisimova, D. Munger, P. Mahautmr, J. X. Tang, M. R. Maxey, and Y. V. Brun, "Accumulation of swimming bacteria near a solid surface," *Phys. Rev. E* **84**, 041932 (2011).
- <sup>48</sup>A. Costanzo, R. D. Leonardo, G. Ruocco, and L. Angelani, "Transport of self-propelling bacteria in micro-channel flow," *J. Phys.: Condens. Matter* **24**, 065101 (2012).
- <sup>49</sup>J. Elgeti and G. Gompper, "Wall accumulation of self-propelled spheres," *Europhys. Lett.* **101**, 48003 (2013).
- <sup>50</sup>R. Bartussek, P. Hänggi, and J. G. Kissner, "Periodically rocked thermal ratchets," *Europhys. Lett.* **28**, 459 (1994).
- <sup>51</sup>P. Hänggi and R. Bartussek, "Brownian rectifiers: How to convert Brownian motion into directed transport," in *Nonlinear Physics of Complex Systems: Current Status and Future Trends* (Springer, 1996), pp. 294–308.
- <sup>52</sup>P. Hänggi and F. Marchesoni, "Artificial brownian motors: Controlling transport on the nanoscale," *Rev. Mod. Phys.* **81**, 387–442 (2009).
- <sup>53</sup>Z. Peng, T. Zhou, and J. F. Brady, "Activity-induced propulsion of a vesicle," *J. Fluid Mech.* **942**, A32 (2022).
- <sup>54</sup>S. Ray, J. Zhang, and Z. Dogic, "Rectified rotational dynamics of mobile inclusions in two-dimensional active nematics," *Phys. Rev. Lett.* **130**, 238301 (2023).
- <sup>55</sup>E. Yariv and O. Schnitzer, "Ratcheting of Brownian swimmers in periodically corrugated channels: A reduced Fokker-Planck approach," *Phys. Rev. E* **90**, 032115 (2014).
- <sup>56</sup>R. Aris, "On the dispersion of a solute in a fluid flowing through a tube," *Proc. R. Soc. A* **235**, 67–77 (1956).
- <sup>57</sup>N. G. Barton, "On the method of moments for solute dispersion," *J. Fluid Mech.* **126**, 205–218 (1983).
- <sup>58</sup>I. Frankel and H. Brenner, "On the foundations of generalized Taylor dispersion theory," *J. Fluid Mech.* **204**, 97–119 (1989).
- <sup>59</sup>H. Brenner and D. A. Edwards, *Macrotransport Processes* (Butterworth-Heinemann, 1993).
- <sup>60</sup>R. Alonso-Matilla, B. Chakrabarti, and D. Saintillan, "Transport and dispersion of active particles in periodic porous media," *Phys. Rev. Fluids* **4**, 043101 (2019).
- <sup>61</sup>W. Jiang and G. Chen, "Dispersion of active particles in confined unidirectional flows," *J. Fluid Mech.* **877**, 1–34 (2019).
- <sup>62</sup>This can be obtained by an argument similar to (30).
- <sup>63</sup>T. Bhattacharjee and S. S. Datta, "Bacterial hopping and trapping in porous media," *Nat. Commun.* **10**, 2075 (2019).
- <sup>64</sup>C. Reichhardt and C. J. O. Reichhardt, "Active matter commensuration and frustration effects on periodic substrates," *Phys. Rev. E* **103**, 022602 (2021).
- <sup>65</sup>M. Kumar, J. S. Guasto, and A. M. Ardekani, "Transport of complex and active fluids in porous media," *J. Rheol.* **66**, 375–397 (2022).
- <sup>66</sup>C. Reichhardt and C. Reichhardt, "Pattern formation and transport for externally driven active matter on periodic substrates," *Europhys. Lett.* **142**, 37001 (2023).
- <sup>67</sup>J.-j. Liao, X.-q. Huang, and B.-q. Ai, "Current reversals of active particles in time-oscillating potentials," *Soft Matter* **14**, 7850–7858 (2018).
- <sup>68</sup>Z. Zhen and G. Pruessner, "Optimal ratchet potentials for run-and-tumble particles," *arXiv:2204.04070* (2022).
- <sup>69</sup>K. J. Modica and S. C. Takatori, "Soft confinement of self-propelled rods: Simulation and theory," *Soft Matter* **20**, 2331–2337 (2024).
- <sup>70</sup>A. R. Dulaney and J. F. Brady, "Waves in active matter: The transition from ballistic to diffusive behavior," *Phys. Rev. E* **101**, 052609 (2020).
- <sup>71</sup>V. A. Shaik, Z. Peng, J. F. Brady, and G. J. Elfring, "Confined active matter in external fields," *Soft Matter* **19**, 1384–1392 (2023).
- <sup>72</sup>W. Yan and J. F. Brady, "Anisotropic swim stress in active matter with nematic order," *New J. Phys.* **20**, 053056 (2018).
- <sup>73</sup>M. J. Schnitzer, "Theory of continuum random walks and application to chemotaxis," *Phys. Rev. E* **48**, 2553–2568 (1993).
- <sup>74</sup>J. Tailleur and M. E. Cates, "Statistical mechanics of interacting run-and-tumble bacteria," *Phys. Rev. Lett.* **100**, 218103 (2008).
- <sup>75</sup>H. Row and J. F. Brady, "Reverse osmotic effect in active matter," *Phys. Rev. E* **101**, 062604 (2020).
- <sup>76</sup>J. Stenhammar, R. Wittkowski, D. Marenduzzo, and M. E. Cates, "Light-induced self-assembly of active rectification devices," *Sci. Adv.* **2**, e1501850 (2016).

- <sup>77</sup>N. A. Söker, S. Auschra, V. Holubec, K. Kroy, and F. Cichos, "How activity landscapes polarize microswimmers without alignment forces," *Phys. Rev. Lett.* **126**, 228001 (2021).
- <sup>78</sup>S. Auschra, V. Holubec, N. A. Söker, F. Cichos, and K. Kroy, "Polarization-density patterns of active particles in motility gradients," *Phys. Rev. E* **103**, 062601 (2021).
- <sup>79</sup>A. Wysocki, A. K. Dasanna, and H. Rieger, "Interacting particles in an activity landscape," *New J. Phys.* **24**, 093013 (2022).
- <sup>80</sup>A. Partovifard, J. Grawitter, and H. Stark, "Controlling active turbulence by activity patterns," *Soft Matter* **20**, 1800 (2024).
- <sup>81</sup>M. E. Cates and J. Tailleur, "Motility-induced phase separation," *Annu. Rev. Condens. Matter Phys.* **6**, 219–244 (2015).
- <sup>82</sup>J. Arlt, V. A. Martinez, A. Dawson, T. Pilizota, and W. C. Poon, "Painting with light-powered bacteria," *Nat. Commun.* **9**, 768 (2018).
- <sup>83</sup>G. Frangipane, D. Dell'Arciprete, S. Petrachini, C. Maggi, F. Saglimbeni, S. Bianchi, G. Vizsnyiczai, M. L. Bernardini, and R. Di Leonardo, "Dynamic density shaping of photokinetic *E. coli*," *eLife* **7**, e36608 (2018).
- <sup>84</sup>F. Hecht, "New development in freefem++," *J. Numer. Math.* **20**, 251–266 (2012).
- <sup>85</sup>K. J. Modica, A. K. Omar, and S. C. Takatori, "Boundary design regulates the diffusion of active matter in heterogeneous environments," *Soft Matter* **19**, 1890–1899 (2023).
- <sup>86</sup>A. Dehkharhani, N. Waisbord, J. Dunkel, and J. S. Guasto, "Bacterial scattering in microfluidic crystal flows reveals giant active Taylor–Aris dispersion," *Proc. Natl. Acad. Sci. U. S. A.* **116**, 11119–11124 (2019).
- <sup>87</sup>M. H. Jacobs and M. Jacobs, *Diffusion Processes* (Springer, 1935).
- <sup>88</sup>R. Zwanzig, "Diffusion past an entropy barrier," *J. Phys. Chem.* **96**, 3926–3930 (1992).
- <sup>89</sup>D. Reguera and J. Rubi, "Kinetic equations for diffusion in the presence of entropic barriers," *Phys. Rev. E* **64**, 061106 (2001).
- <sup>90</sup>P. Kalinay and J. K. Percus, "Projection of two-dimensional diffusion in a narrow channel onto the longitudinal dimension," *J. Chem. Phys.* **122**, 204701 (2005).
- <sup>91</sup>D. Reguera, G. Schmid, P. S. Burada, J. Rubi, P. Reimann, and P. Hägggi, "Entropic transport: Kinetics, scaling, and control mechanisms," *Phys. Rev. Lett.* **96**, 130603 (2006).
- <sup>92</sup>P. Kalinay and J. K. Percus, "Approximations of the generalized Fick-Jacobs equation," *Phys. Rev. E* **78**, 021103 (2008).
- <sup>93</sup>P. S. Burada, G. Schmid, D. Reguera, J. Rubi, and P. Hägggi, "Biased diffusion in confined media: Test of the Fick-Jacobs approximation and validity criteria," *Phys. Rev. E* **75**, 051111 (2007).
- <sup>94</sup>Z. Peng and J. F. Brady, "Trapped-particle microrheology of active suspensions," *J. Chem. Phys.* **157**, 104119 (2022).
- <sup>95</sup>S.-c. Lu, Y.-l. Ou, and B.-q. Ai, "Ratchet transport of an active–passive mixture chain in confined structures," *Physica A* **482**, 501–506 (2017).
- <sup>96</sup>D. Debnath, P. K. Ghosh, V. R. Misko, Y. Li, F. Marchesoni, and F. Nori, "Enhanced motility in a binary mixture of active nano/microswimmers," *Nanoscale* **12**, 9717–9726 (2020).
- <sup>97</sup>C. Wang and H. Jiang, "Different-shaped micro-objects driven by active particle aggregations," *Soft Matter* **16**, 4422–4430 (2020).
- <sup>98</sup>Z. Wang and J. Hao, "Controlling the transport of the mixture involving active and passive rods in confined channel," *Soft Matter* **19**, 6368–6375 (2023).
- <sup>99</sup>L. Angelani and R. D. Leonardo, "Geometrically biased random walks in bacteria-driven micro-shuttles," *New J. Phys.* **12**, 113017 (2010).
- <sup>100</sup>S. Belan and M. Kardar, "Active motion of passive asymmetric dumbbells in a non-equilibrium bath," *J. Chem. Phys.* **154**, 024109 (2021).
- <sup>101</sup>P. Dolai, A. S. Rajput, and K. V. Kumar, "Shape-dependent motility of polar inclusions in active baths," *Phys. Rev. E* **110**, 014607 (2024).
- <sup>102</sup>P. Pietzonka, É. Fodor, C. Lohrmann, M. E. Cates, and U. Seifert, "Autonomous engines driven by active matter: Energetics and design principles," *Phys. Rev. X* **9**, 041032 (2019).